

Isospin-breaking effects in the three-pion contribution to hadronic vacuum polarization

Martin Hoferichter,^a Bai-Long Hoid,^a Bastian Kubis,^b and Dominic Schuh^b

^a*Albert Einstein Center for Fundamental Physics, Institute for Theoretical Physics, University of Bern, Sidlerstrasse 5, 3012 Bern, Switzerland*

^b*Helmholtz-Institut für Strahlen- und Kernphysik (Theorie) and Bethe Center for Theoretical Physics, Universität Bonn, 53115 Bonn, Germany*

E-mail: hoferichter@itp.unibe.ch, longbai@itp.unibe.ch,
kubis@hiskp.uni-bonn.de, schuh@hiskp.uni-bonn.de

ABSTRACT: Isospin-breaking (IB) effects are required for an evaluation of hadronic vacuum polarization at subpercent precision. While the dominant contributions arise from the $e^+e^- \rightarrow \pi^+\pi^-$ channel, also IB in the subleading channels can become relevant for a detailed understanding, e.g., of the comparison to lattice QCD. Here, we provide such an analysis for $e^+e^- \rightarrow 3\pi$ by extending our dispersive description of the process, including estimates of final-state radiation (FSR) and ρ - ω mixing. In particular, we develop a formalism to capture the leading infrared-enhanced effects in terms of a correction factor $\eta_{3\pi}$ that generalizes the analog treatment of virtual and final-state photons in the 2π case. The global fit to the $e^+e^- \rightarrow 3\pi$ data base, subject to constraints from analyticity, unitarity, and the chiral anomaly, gives $a_\mu^{3\pi}|_{\leq 1.8\text{ GeV}} = 45.91(53) \times 10^{-10}$ for the total 3π contribution to the anomalous magnetic moment of the muon, of which $a_\mu^{\text{FSR}}[3\pi] = 0.51(1) \times 10^{-10}$ and $a_\mu^{\rho-\omega}[3\pi] = -2.68(70) \times 10^{-10}$ can be ascribed to IB. We argue that the resulting cancellation with ρ - ω mixing in $e^+e^- \rightarrow 2\pi$ can be understood from a narrow-resonance picture, and provide updated values for the vacuum-polarization-subtracted vector-meson parameters $M_\omega = 782.70(3)$ MeV, $M_\phi = 1019.21(2)$ MeV, $\Gamma_\omega = 8.71(3)$ MeV, and $\Gamma_\phi = 4.27(1)$ MeV.

Contents

1	Introduction	1
2	Dispersive parameterization of $e^+e^- \rightarrow 3\pi$	3
3	Electromagnetic corrections to $e^+e^- \rightarrow 3\pi$	5
4	ρ-ω mixing in $e^+e^- \rightarrow 3\pi$	8
5	Fits to $e^+e^- \rightarrow 3\pi$ data	11
5.1	Fits to data base prior to BaBar 2021	11
5.2	Fits to BaBar 2021	14
5.3	Global fit	16
6	Consequences for the anomalous magnetic moment of the muon	20
7	Conclusions	20

1 Introduction

A detailed understanding of hadronic vacuum polarization (HVP) is critical for the interpretation of the anomalous magnetic moment of the muon $a_\mu = (g - 2)_\mu/2$ [1–5],

$$a_\mu^{\text{exp}} = 116\,592\,061(41) \times 10^{-11}, \quad (1.1)$$

given that the uncertainty in the Standard-Model (SM) prediction [6–33],

$$a_\mu^{\text{SM}}[e^+e^-] = 116\,591\,810(43) \times 10^{-11}, \quad (1.2)$$

is dominated by the uncertainties propagated from $e^+e^- \rightarrow$ hadrons cross sections. Moreover, while for the second-most-important hadronic contribution, hadronic light-by-light scattering, subsequent studies in lattice QCD [34–38] and using data-driven methods [39–50] point towards a consistent picture in line with the evaluation from Ref. [6] and on track to meet the precision requirements of the Fermilab experiment [51, 52], various tensions persist for the case of HVP.¹

First, the global HVP integral from the lattice-QCD evaluation of Ref. [55] differs from e^+e^- data [6] by 2.1σ . Confirmation by other lattice-QCD collaborations for the entire integral is still pending, but the stronger tension in a partial quantity, the intermediate window [56], has been established by several independent calculations [57–61]. Second, new $e^+e^- \rightarrow$ hadrons data have become available since Ref. [6], including the crucial $e^+e^- \rightarrow 2\pi$

¹Higher-order hadronic corrections [18, 33, 53, 54] are already under sufficient control.

channel. Here, the measurement by SND20 [62] comports with previous experiments, but the result by CMD-3 [63] differs from CMD-2 [64], SND05 [65], BaBar [66], KLOE [67], and BESIII [68], at a combined level of 5σ .

Neither of these tensions are currently understood, and the patterns in which the deviations occur do not point to a simple solution.² That is, the relative size of the deviations in the intermediate window and the total HVP integral, together with the consequences for the hadronic running of the fine-structure constant [73–78], indicates that the changes in the cross section cannot be contained to the 2π channel alone, but that some component at intermediate energies beyond 1 GeV in center-of-mass energy is required. Besides further scrutiny of $e^+e^- \rightarrow \pi^+\pi^-$ [79–81], this motivates the consideration of subleading channels such as $e^+e^- \rightarrow 3\pi$ [14] and $e^+e^- \rightarrow \bar{K}K$ [82], which, in combination with more calculations of window observables or related quantities [83], could help locate the origin of the tensions.

In addition, the detailed comparison to lattice QCD requires the calculation of isospin-breaking (IB) effects and other subleading corrections to the isosymmetric, quark-connected correlators. The sum of the dominant IB effects from 2π , $\bar{K}K$, and the radiative channels $\pi^0\gamma$, $\eta\gamma$ [84] agrees reasonably well with Ref. [55], but in the context of strong IB a larger result was observed, more in line with an inclusive estimate from chiral perturbation theory (ChPT) [85]. Albeit consistent within uncertainties, it thus seems prudent to extend the analysis to IB in $e^+e^- \rightarrow 3\pi$, especially, since the BaBar analysis [86] reports a signal for ρ – ω mixing, an effect dominated by strong IB. Apart from the direct comparison to lattice QCD, such IB corrections are also of interest for an indirect, data-driven determination of quark-disconnected contributions [87–89].

In this work, we address the two main IB effects in $e^+e^- \rightarrow 3\pi$. First, we study the role of radiative corrections, with the aim to provide a correction factor analogous to $\eta_{2\pi}(s)$ in $e^+e^- \rightarrow 2\pi$ [90–93] that quantifies the combined correction due to virtual photons and final-state radiation (FSR) as a function of the center-of-mass energy of the process. Given that already the leading order in ChPT is determined by the Wess–Zumino–Witten (WZW) anomaly [94, 95], whose derivative structure mandates the inclusion of contact terms to render loop corrections UV finite [96–98], a complete treatment that captures all low-energy terms at $\mathcal{O}(\alpha)$ while, at the same time, accounting for the resonance physics of the process becomes a formidable challenge. Instead, we make use of the observation from Ref. [99] in the context of $e^+e^- \rightarrow \pi\pi(\gamma)$, i.e., that by far the most relevant numerical effect arises from the infrared (IR) enhanced contributions that survive after the cancellation of IR singularities between virtual and bremsstrahlung diagrams. We set up a framework that allows us to evaluate these corrections using as input basis function for a Khuri–Treiman (KT) treatment of $\gamma^* \rightarrow 3\pi$ [100], and extrapolate the resulting correction factor $\eta_{3\pi}(s)$ to the 3π threshold by means of a non-relativistic (NR) expansion. After a review of our dispersive representation for $e^+e^- \rightarrow 3\pi$ in Sec. 2, this formalism is presented in Sec. 3.

The second major IB effect is generated by ρ – ω mixing. On the one hand, this effect

²Explanations in terms of physics beyond the SM have been considered [69–72], but rather elaborate constructions would be required to evade other constraints on the parameter space.

is expected to be enhanced compared to $e^+e^- \rightarrow 2\pi$ since the ω couples more weakly to the electromagnetic current than the ρ —in a vector-meson-dominance (VMD) picture by a relative factor 3, which thus translates to almost an order of magnitude in the ρ – ω mixing contribution. On the other hand, the large width of the ρ makes the effect much less localized than in the 2π system, in such a way that the resulting integral becomes more sensitive to the assumed line shape, and care is required to differentiate an IB effect from background contributions to the cross section. To parameterize the line shape in a way consistent with the definition of the mixing parameter ϵ_ω as a residue in $e^+e^- \rightarrow 2\pi$, we follow the coupled-channel formalism from Ref. [46], with the main features summarized in Sec. 4. Updated fits to the $e^+e^- \rightarrow 3\pi$ data base are presented in Sec. 5, the consequences for a_μ in Sec. 6. We summarize our results in Sec. 7.

2 Dispersive parameterization of $e^+e^- \rightarrow 3\pi$

As starting point for the study of IB effects, we use the dispersive representation of the $e^+e^- \rightarrow 3\pi$ cross section from Ref. [14], first derived in the context of the pion transition form factor [26, 27, 101]. The key idea amounts to combining the normalization from the WZW anomaly in terms of the pion decay constant F_π [102–104] with a calculation of the $\pi\pi$ rescattering corrections in the KT formalism, generalizing work on $\omega, \phi \rightarrow 3\pi$ decays [105–110] to arbitrary photon virtualities $\gamma^* \rightarrow 3\pi$.

The general expression of the matrix element for $\gamma^*(q) \rightarrow \pi^+(p_+)\pi^-(p_-)\pi^0(p_0)$ is given by

$$\langle 0|j_\mu(0)|\pi^+(p_+)\pi^-(p_-)\pi^0(p_0)\rangle = -\epsilon_{\mu\nu\alpha\beta}p_+^\nu p_-^\alpha p_0^\beta \mathcal{F}(s, t, u; q^2), \quad (2.1)$$

with $q = p_+ + p_- + p_0$, $s = (p_+ + p_-)^2$, $t = (p_- + p_0)^2$, $u = (p_+ + p_0)^2$, and $s + t + u = 3M_\pi^2 + q^2$. We further decompose the invariant function \mathcal{F} as

$$\mathcal{F}(s, t, u; q^2) = \mathcal{F}(s, q^2) + \mathcal{F}(t, q^2) + \mathcal{F}(u, q^2), \quad (2.2)$$

and perform a partial-wave expansion, where due to Bose symmetry only odd partial waves contribute [111]

$$\mathcal{F}(s, t, u; q^2) = \sum_{\ell \text{ odd}} f_\ell(s, q^2) P'_\ell(z_s). \quad (2.3)$$

The kinematic quantities are

$$z_s = \cos \theta_s = \frac{t - u}{\kappa(s, q^2)}, \quad \kappa(s, q^2) = \sigma_\pi(s) \lambda^{1/2}(q^2, M_\pi^2, s),$$

$$\lambda(x, y, z) = x^2 + y^2 + z^2 - 2(xy + yz + xz), \quad \sigma_\pi(s) = \sqrt{1 - \frac{4M_\pi^2}{s}}, \quad (2.4)$$

and $P'_\ell(z)$ denotes the derivatives of the Legendre polynomials. The decomposition (2.2) strictly applies as long as the discontinuities of F - and higher partial waves are negligible, as well justified below the onset of the $\rho_3(1690)$ resonance [14, 106, 112]. The resulting cross section is expressed as the integral

$$\sigma_{e^+e^- \rightarrow 3\pi}(q^2) = \alpha^2 \int_{s_{\min}}^{s_{\max}} ds \int_{t_{\min}}^{t_{\max}} dt \frac{s[\kappa(s, q^2)]^2(1 - z_s^2)}{768 \pi q^6} |\mathcal{F}(s, t, u; q^2)|^2, \quad (2.5)$$

with integration boundaries

$$\begin{aligned} s_{\min} &= 4M_\pi^2, & s_{\max} &= (\sqrt{q^2} - M_\pi)^2, \\ t_{\min/\max} &= (E_-^* + E_0^*)^2 - \left(\sqrt{E_-^{*2} - M_\pi^2} \pm \sqrt{E_0^{*2} - M_\pi^2} \right)^2, \end{aligned} \quad (2.6)$$

and

$$E_-^* = \frac{\sqrt{s}}{2}, \quad E_0^* = \frac{q^2 - s - M_\pi^2}{2\sqrt{s}}. \quad (2.7)$$

The momentum dependence of the partial wave $f_1(s, q^2)$ is then predicted from the KT formalism up to an overall normalization $a(q^2)$, which we parameterize following the same ansatz as in Ref. [14]

$$a(q^2) = \alpha_A + \frac{q^2}{\pi} \int_{s_{\text{thr}}}^{\infty} ds' \frac{\text{Im} \mathcal{A}(s')}{s'(s' - q^2)} + C_p(q^2). \quad (2.8)$$

The three terms correspond to the WZW normalization, resonance contributions (most notably ω and ϕ , but also $\omega'(1420)$, $\omega''(1650)$) to be able to describe the data up to 1.8 GeV), and a conformal polynomial to parameterize non-resonant contributions. For the WZW normalization, the best estimate is still given by [108, 113]

$$\alpha_A = \frac{F_{3\pi}}{3} \times 1.066(10), \quad F_{3\pi} = \frac{1}{4\pi^2 F_\pi^3}, \quad (2.9)$$

a low-energy theorem that could be tested with future lattice-QCD calculations [114–116]. The resonant contributions are described by taking the imaginary part from

$$\mathcal{A}(q^2) = \sum_V \frac{c_V}{M_V^2 - q^2 - i\sqrt{q^2} \Gamma_V(q^2)}. \quad (2.10)$$

The energy-dependent widths $\Gamma_V(q^2)$ for $V = \omega, \phi$ include the main decay channels, in particular, $\omega \rightarrow \pi^0 \gamma$ sets the integration threshold to $s_{\text{thr}} = M_{\pi^0}^2$. For the 3π channel, the partial width accounts for the 3π rescattering as well, and the remaining tiny effects from the neglected channels $\omega \rightarrow 2\pi$ and $\phi \rightarrow \eta \gamma$ are corrected by a rescaling of the partial widths. ω' and ω'' are assumed to exclusively decay to 3π for simplicity. As before, we fix the ω'' parameters to the PDG values [117], but for ω' we observe that our fits do become sensitive to the assumption for the mass parameter, and thus introduce $M_{\omega'}$ as an additional degree of freedom in our representation. The conformal polynomial,

$$C_p(q^2) = \sum_{i=1}^p c_i (z(q^2)^i - z(0)^i), \quad z(q^2) = \frac{\sqrt{s_{\text{inel}} - s_1} - \sqrt{s_{\text{inel}} - q^2}}{\sqrt{s_{\text{inel}} - s_1} + \sqrt{s_{\text{inel}} - q^2}}, \quad (2.11)$$

is unchanged compared to Ref. [14]: $s_{\text{inel}} = 1 \text{ GeV}^2$, $s_1 = -1 \text{ GeV}^2$, and the absence of an S -wave cusp as well as the sum rule for α_A are imposed as additional constraints on $C_p(q^2)$.

3 Electromagnetic corrections to $e^+e^- \rightarrow 3\pi$

In the 2π channel, the effect of radiative corrections on the total cross section is often estimated using “FsQED,” i.e., scalar QED dressed with the pion form factor F_π^V . In a dispersive picture, this approach amounts to isolating pion-pole contributions and replacing the constant $\pi\pi\gamma$ coupling as predicted in scalar QED by the full matrix element. This procedure captures the IR-enhanced contributions, which provide the dominant effect compared to non-pion-pole $\pi\pi\gamma$ states [99], leading to a universal correction factor

$$\sigma_{e^+e^- \rightarrow 2\pi(\gamma)}(q^2) = \sigma_{e^+e^- \rightarrow 2\pi}^{(0)}(q^2) \left(1 + \frac{\alpha}{\pi} \eta_{2\pi}(q^2)\right), \quad \sigma_{e^+e^- \rightarrow 2\pi}^{(0)}(q^2) = \frac{\pi\alpha^2}{3q^2} \sigma_\pi^3(q^2) |F_\pi^V(q^2)|^2, \quad (3.1)$$

with [90–93]

$$\begin{aligned} \eta_{2\pi}(s) &= \frac{3(1 + \sigma_\pi^2(s))}{2\sigma_\pi^2(s)} - 4 \log \sigma_\pi(s) + 6 \log \frac{1 + \sigma_\pi(s)}{2} + \frac{1 + \sigma_\pi^2(s)}{\sigma_\pi(s)} F(\sigma_\pi(s)) \\ &\quad - \frac{(1 - \sigma_\pi(s))(3 + 3\sigma_\pi(s) - 7\sigma_\pi^2(s) + 5\sigma_\pi^3(s))}{4\sigma_\pi^3(s)} \log \frac{1 + \sigma_\pi(s)}{1 - \sigma_\pi(s)}, \\ F(x) &= -4\text{Li}_2(x) + 4\text{Li}_2(-x) + 2 \log x \log \frac{1+x}{1-x} + 3\text{Li}_2\left(\frac{1+x}{2}\right) - 3\text{Li}_2\left(\frac{1-x}{2}\right) + \frac{\pi^2}{2}, \\ \text{Li}_2(x) &= - \int_0^x dt \frac{\log(1-t)}{t}. \end{aligned} \quad (3.2)$$

For the 2π channel, the role of radiative corrections beyond the FsQED approximation is an active subject of discussion [79, 118–121], especially in view of the CMD-3 measurement [63], but for $e^+e^- \rightarrow 3\pi$ so far no robust estimates of radiative corrections are available at all, which strongly motivates the focus on the IR-enhanced effects as the numerically dominant contribution.

To isolate these effects, we proceed as follows: even when neglecting the discontinuities of $\ell \geq 3$ partial waves, the full amplitude receives contributions beyond P -waves from the projection of the crossed-channel amplitudes, i.e.,

$$f_1(s, q^2) = \mathcal{F}(s, q^2) + \hat{\mathcal{F}}(s, q^2), \quad (3.3)$$

where

$$\hat{\mathcal{F}}(s, q^2) = \frac{3}{2} \int_{-1}^1 dz_s (1 - z_s^2) \mathcal{F}(t(s, q^2, z_s), q^2). \quad (3.4)$$

For the pure P -wave subsystem, the combination of the IR-enhanced virtual-photon and bremsstrahlung diagrams reproduces the functional form of $\eta_{2\pi}$ as given in Eq. (3.2), with the momentum not determined by the e^+e^- invariant mass q^2 , but by the invariant mass

of the $\pi^+\pi^-$ subsystem. Accordingly, we can capture this effect by writing

$$\begin{aligned} \sigma_{e^+e^- \rightarrow 3\pi(\gamma)}(q^2) &\propto \int_{s_{\min}}^{s_{\max}} ds \int_{t_{\min}}^{t_{\max}} dt s [\kappa(s, q^2)]^2 (1 - z_s^2) \\ &\times \left| \underbrace{(\mathcal{F}(s, q^2) + \hat{\mathcal{F}}(s, q^2))}_{f_1(s, q^2)} \sqrt{1 + \frac{\alpha}{\pi} \eta_{2\pi}(s)} \right. \\ &\quad \left. + \underbrace{(\mathcal{F}(t, q^2) + \mathcal{F}(u, q^2) - \hat{\mathcal{F}}(s, q^2))}_{f_3(s, q^2) + \dots} \sqrt{1 + \frac{\alpha}{\pi} \eta_{2\pi}(s_{\text{PT}})} \right|^2, \end{aligned} \quad (3.5)$$

where all factors that drop out in

$$1 + \frac{\alpha}{\pi} \eta_{3\pi}(q^2) = \frac{\sigma_{e^+e^- \rightarrow 3\pi(\gamma)}(q^2)}{\sigma_{e^+e^- \rightarrow 3\pi}^{(0)}(q^2)} \quad (3.6)$$

have been ignored and $s_{\text{PT}} = (\sqrt{q^2} - M_\pi)^2$ denotes the position of the pseudothreshold. This kinematic point is critical, since $\hat{\mathcal{F}}(s, q^2)$ diverges at s_{PT} , in such a way that the crossed-channel contribution starting at $\ell = 3$ needs to be multiplied by a function that ensures that the cancellation at s_{PT} is maintained in the presence of radiative corrections. The choice of this kinematic function is not unique, in Eq. (3.5) we show the minimal variant in which a constant correction is assumed. However, the ambiguity in this correction only affects higher partial waves, and by definition cannot contribute to the IR-enhanced effects in the P -wave subsystem. For this reason, we may choose to evaluate this correction factor at s instead of s_{PT} , which simplifies the result to

$$\begin{aligned} \sigma_{e^+e^- \rightarrow 3\pi(\gamma)}(q^2) &\propto \int_{s_{\min}}^{s_{\max}} ds \int_{t_{\min}}^{t_{\max}} dt s [\kappa(s, q^2)]^2 (1 - z_s^2) \\ &\times \left| \mathcal{F}(s, q^2) + \mathcal{F}(t, q^2) + \mathcal{F}(u, q^2) \right|^2 \left(1 + \frac{\alpha}{\pi} \eta_{2\pi}(s) \right). \end{aligned} \quad (3.7)$$

We checked that both variants indeed lead to minor differences, and will continue to work with Eq. (3.7) in the following. For the numerical evaluation of Eq. (3.6) we use the KT basis functions from Ref. [122].

In analogy to $\eta_{2\pi}$, the correction factor $\eta_{3\pi}(q^2)$ involves a Coulomb divergence at threshold $\propto (q^2 - 9M_\pi^2)^{-1/2}$,³ so that for the application in fits to $e^+e^- \rightarrow 3\pi$ cross-section data it is convenient to provide numerical results for

$$\bar{\eta}_{3\pi}(q^2) = \eta_{3\pi}(q^2) \sqrt{1 - \frac{9M_\pi^2}{q^2}}. \quad (3.8)$$

Moreover, the numerical solution of the KT equations becomes unstable close to threshold, making the determination of the coefficient of the Coulomb divergence by other means

³We emphasize that the Coulomb divergence $\propto (s - 4M_\pi^2)^{-1/2}$ is present in Eq. (3.7) for every q^2 . However, after integration over s and t , this translates into a divergence in q^2 only at the three-pion threshold.

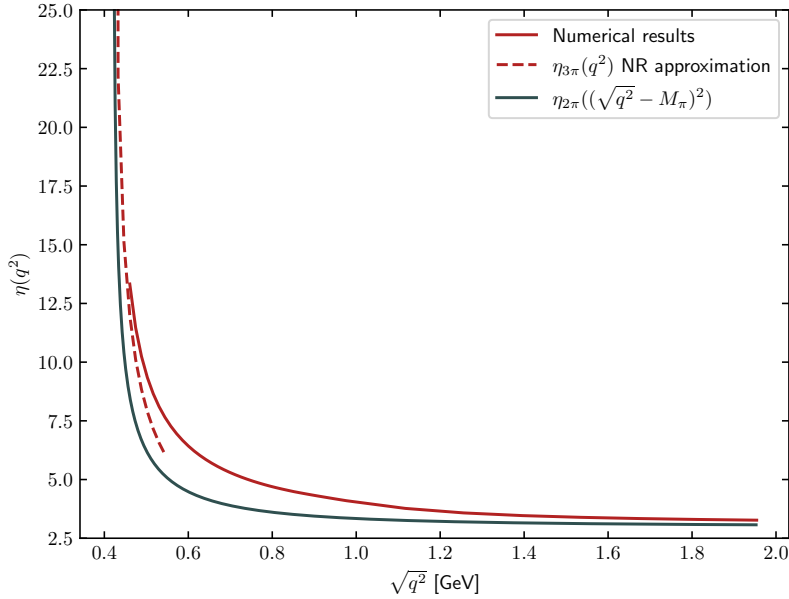


Figure 1. Comparison of the numerical result for $\eta_{3\pi}$ (red solid), its NR approximation (red dashed), and $\eta_{2\pi}$ shifted to the 3π threshold (blue solid).

valuable to be able to interpolate to the range starting at $\sqrt{q^2} \approx 3.3M_\pi$ where a numerical solution is feasible. This can be achieved by a NR expansion. Starting from

$$\eta_{2\pi}(s) = \frac{\pi^2}{2\sigma_\pi(s)} - 2 + \mathcal{O}(\sigma_\pi), \quad (3.9)$$

we perform the substitution $s = 4M_\pi^2(1-x) + (\sqrt{q^2} - M_\pi)^2x$ and expand $\sqrt{q^2} = 3M_\pi(1+\epsilon)$ around threshold. The t integration and $\mathcal{F}(s, q^2) + \mathcal{F}(t, q^2) + \mathcal{F}(u, q^2)$ can be ignored as they cancel in the ratio, while the remaining kinematic dependence leads to

$$\eta_{3\pi}(\epsilon) = \frac{256\pi}{105\sqrt{3}\epsilon} - 2 + \mathcal{O}(\sqrt{\epsilon}), \quad (3.10)$$

and therefore

$$\bar{\eta}_{3\pi}(9M_\pi^2) = \frac{256\pi}{105} \sqrt{\frac{2}{3}}. \quad (3.11)$$

The numerical result for $\eta_{3\pi}$ is shown in Fig. 1, in comparison to the NR approximation and $\eta_{2\pi}$ shifted to the 3π threshold. From this comparison it follows that $\eta_{3\pi}$ is really distinctly different from $\eta_{2\pi}$, reflected by the increase that is observed in addition to the change of threshold. In Fig. 2, we also show the result for $\bar{\eta}_{3\pi}$, as we will use in the implementation together with the threshold factor in Eq. (3.8).

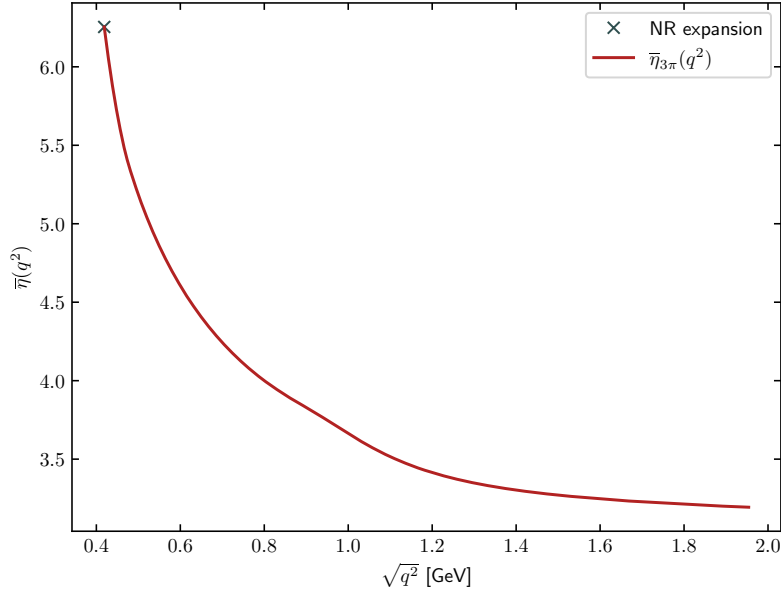


Figure 2. 3π FSR factor $\bar{\eta}_{3\pi}$, with the threshold divergence removed according to Eq. (3.8) (the result is available as text file in the supplementary material).

4 ρ - ω mixing in $e^+e^- \rightarrow 3\pi$

ρ - ω mixing in $e^+e^- \rightarrow 2\pi$ can be implemented via a correction factor [81]

$$\begin{aligned}
 G_\omega(s) = & 1 + \frac{s}{\pi} \int_{9M_\pi^2}^{\infty} ds' \frac{\text{Re } \epsilon_\omega}{s'(s'-s)} \text{Im} \left[\frac{s'}{(M_\omega - \frac{i}{2}\Gamma_\omega)^2 - s'} \right] \left(\frac{1 - \frac{9M_\pi^2}{s'}}{1 - \frac{9M_\pi^2}{M_\omega^2}} \right)^4 \\
 & + \frac{s}{\pi} \int_{M_{\pi^0}^2}^{\infty} ds' \frac{\text{Im } \epsilon_\omega}{s'(s'-s)} \text{Re} \left[\frac{s'}{(M_\omega - \frac{i}{2}\Gamma_\omega)^2 - s'} \right] \left(\frac{1 - \frac{M_{\pi^0}^2}{s'}}{1 - \frac{M_{\pi^0}^2}{M_\omega^2}} \right)^3, \quad (4.1)
 \end{aligned}$$

which amounts to a dispersively improved variant of a Breit–Wigner ansatz

$$g_\omega(s) = 1 + \frac{\epsilon_\omega s}{M_\omega^2 - s - iM_\omega\Gamma_\omega} \quad (4.2)$$

that, besides removing the unphysical imaginary part below the 3π threshold, also allows for the $\pi^0\gamma$ cut and thus an IB phase in ϵ_ω . In particular, Eq. (4.1) shows that ρ - ω mixing in $e^+e^- \rightarrow 2\pi$ is intimately related to the residue at the ω pole, since the small width of the ω , together with the threshold and asymptotic constraints on the line shape, leaves little freedom in the construction of $G_\omega(s)$.

In contrast, ρ - ω mixing in $e^+e^- \rightarrow 3\pi$ is far less localized, and due to the large width of the ρ a significant sensitivity to the assumed line shape off the resonance is expected. In particular, the absence of sharp interference features in the cross section could potentially

lead one to misidentify a non-resonant background as an IB contribution. To mitigate such effects, we use the line shape as predicted by the coupled-channel formalism from Ref. [46] for e^+e^- , $\pi^+\pi^-$, and 3π , constructed for a consistent implementation of ρ - ω mixing in $e^+e^- \rightarrow 2\pi$, $\eta' \rightarrow \pi^+\pi^-\gamma$, and the η' transition form factor. The main idea follows Ref. [123] (see also Refs. [124, 125]): the full multichannel scattering amplitude arises from iterating a scattering potential via self energies, combined with elastic $\pi\pi$ rescattering as described by the Omnès function [126] in a way that is consistent with analyticity and unitarity. Including the photon and ω poles in the resonance potential, the formalism then predicts the shape of the amplitudes in the various channels that follows from a dispersive representation of the self energies together with the multichannel dynamics.

As a first step, the formalism reproduces the vacuum polarization (VP) function

$$\Pi(s) = \Pi_e(s) + \Pi_\pi(s) \left(1 + \frac{2s\epsilon_\omega}{M_\omega^2 - s - iM_\omega\Gamma_\omega} \right) + \Pi_\omega(s) + \mathcal{O}(\epsilon_\omega^2), \quad (4.3)$$

where the ω contribution is represented in a narrow-width approximation

$$\Pi_\omega(s) = \frac{1}{g_{\omega\gamma}^2} \frac{e^2 s}{s - M_\omega^2 + iM_\omega\Gamma_\omega}, \quad (4.4)$$

while the ρ remains resolved as a 2π resonance

$$\Pi_\pi(s) = -\frac{e^2 s}{48\pi^2} \int_{4M_\pi^2}^{\infty} ds' \frac{\sigma_\pi^3(s') |F_\pi^V(s')|^2}{s'(s' - s - i\epsilon)}. \quad (4.5)$$

$\Pi_e(s)$ in Eq. (4.3) gives the leptonic VP, and ρ - ω mixing is represented by a product of $\Pi_\pi(s)$ with the narrow-width ω propagator. For $\Gamma_\rho \rightarrow 0$, $\Pi_\pi(s)$ collapses to

$$\Pi_\pi(s) \rightarrow \Pi_\rho(s) = \frac{1}{g_{\rho\gamma}^2} \frac{e^2 s}{s - M_\rho^2 + iM_\rho\Gamma_\rho}. \quad (4.6)$$

The couplings introduced in Eqs. (4.4) and (4.6) are related to the dilepton decay $V \rightarrow e^+e^-$ via $\Gamma_{V \rightarrow e^+e^-} = 4\pi\alpha^2 M_V / (3|g_{V\gamma}|^2)$; numerically, we will use $|g_{\omega\gamma}| = 16.2(8)$ [46] and $|g_{\rho\gamma}| = 4.9(1)$ [112], where the latter determination invokes an analytic continuation to the ρ pole instead of a narrow-resonance estimate on the real axis. The deviation of $|g_{\omega\gamma}|/|g_{\rho\gamma}| = 3.3(2)$ from 3 quantifies the deviation from the VMD expectation in these couplings.

Most importantly, the same formalism also reproduces Eq. (4.2) for ρ - ω mixing in $e^+e^- \rightarrow 2\pi$, and predicts the analog correction for $e^+e^- \rightarrow 3\pi$ [46]

$$g_\pi(s) = 1 - \frac{g_{\omega\gamma}^2 \epsilon_\omega}{e^2} \Pi_\pi(s). \quad (4.7)$$

In the narrow-width limit (4.6) one thus finds the exact same form apart from $\epsilon_\omega \rightarrow \epsilon_\omega g_{\omega\gamma}^2 / g_{\rho\gamma}^2$, and thus the VMD enhancement factor expected from the smaller photon coupling of the ω .⁴ However, instead of having to rely on a narrow-width approximation for the

⁴In the typical conventions [127, 128], the coupling strength is proportional to $1/g_{V\gamma}$.

ρ , we can use the full result (4.7), which ensures that the mixing parameter ϵ_ω is defined in a way consistent with $e^+e^- \rightarrow 2\pi$, and that the line shape correctly implements the dispersion relation for the two-pion self energy. In practice, we will use Eq. (4.5) with ρ - ω mixing in $F_\pi^V(s)$ switched off, given that such higher-order IB effects cannot be described in a consistent manner.

From similar arguments, we can glean some intuition about the size of IB to be expected in the different channels when inserted into the HVP integral. To this end, we write the HVP master formula as [129, 130]

$$a_\mu^{\text{HVP}} = \left(\frac{\alpha m_\mu}{3\pi}\right)^2 \int_{s_{\text{thr}}}^\infty ds \frac{\hat{K}(s)}{s^2} R_{\text{had}}(s) = -\left(\frac{\alpha m_\mu}{3\pi}\right)^2 \int_{s_{\text{thr}}}^\infty ds \frac{\hat{K}(s)}{s^2} \frac{12\pi}{e^2} \text{Im} \Pi(s), \quad (4.8)$$

with

$$\hat{K}(s) = \frac{3s}{m_\mu^2} \left[\frac{x^2}{2} (2 - x^2) + \frac{(1+x^2)(1+x)^2}{x^2} \left(\log(1+x) - x + \frac{x^2}{2} \right) + \frac{1+x}{1-x} x^2 \log x \right],$$

$$x = \frac{1 - \sigma_\mu(s)}{1 + \sigma_\mu(s)}, \quad \sigma_\mu(s) = \sqrt{1 - \frac{4m_\mu^2}{s}}. \quad (4.9)$$

In the narrow-width limit, one thus finds

$$a_\mu^\rho = \left(\frac{\alpha m_\mu}{3\pi}\right)^2 \frac{\hat{K}(M_\rho^2)}{M_\rho^2} \frac{12\pi^2}{|g_{\rho\gamma}|^2} \simeq 482 \times 10^{-10},$$

$$a_\mu^\omega = \left(\frac{\alpha m_\mu}{3\pi}\right)^2 \frac{\hat{K}(M_\omega^2)}{M_\omega^2} \frac{12\pi^2}{|g_{\omega\gamma}|^2} \simeq 43.6 \times 10^{-10}, \quad (4.10)$$

both within a few percent of the expected contribution when integrating around the ρ and ω resonances in the 2π and 3π cross sections, respectively. Based on Eq. (4.3), the ρ - ω mixing contribution becomes

$$a_\mu^{\rho-\omega} = \left(\frac{\alpha m_\mu}{3\pi}\right)^2 \int_{s_{\text{thr}}}^\infty ds \hat{K}(s) \frac{24\pi\epsilon_\omega}{|g_{\rho\gamma}|^2} \text{Im} \left[\frac{1}{s - M_\rho^2 + iM_\rho\Gamma_\rho} \frac{1}{s - M_\omega^2 + iM_\omega\Gamma_\omega} \right]. \quad (4.11)$$

This expression is of course rather sensitive to integration range and line shape, clearly, for such a subtle interference a narrow-width approximation for the ρ is not adequate. Still, it is striking that the numerical evaluation of Eq. (4.11) produces $|a_\mu^{\rho-\omega}| \lesssim 0.5 \times 10^{-10}$, while even a simple narrow-width formula such as Eq. (4.6) for $F_\pi^V(s)$ multiplied with Eq. (4.2) gives results for the ρ - ω contribution in the 2π channel much closer to the detailed analysis of Ref. [81]. Ultimately, this behavior seems to arise because the entire ρ - ω mixing effect from Eq. (4.3) should not be attributed to the 2π channel alone, instead, a partial-fraction decomposition

$$\frac{1}{s - M_\rho^2 + iM_\rho\Gamma_\rho} \frac{1}{s - M_\omega^2 + iM_\omega\Gamma_\omega} = \frac{1}{M_\rho^2 - M_\omega^2 - iM_\rho\Gamma_\rho + iM_\omega\Gamma_\omega}$$

$$\times \left(\frac{1}{s - M_\rho^2 + iM_\rho\Gamma_\rho} - \frac{1}{s - M_\omega^2 + iM_\omega\Gamma_\omega} \right) \quad (4.12)$$

suggests that a ρ - ω mixing contribution should arise in both the 2π and 3π channel, and while the detailed phenomenology will again crucially depend on the line shape, evaluating both terms in Eq. (4.12) separately in the integral (4.11) does produce sizable cancellations. From this perspective, at least a partial cancellation of the ρ - ω mixing contributions in the actual $e^+e^- \rightarrow 2\pi$ and $e^+e^- \rightarrow 3\pi$ cross sections would not appear surprising.

5 Fits to $e^+e^- \rightarrow 3\pi$ data

5.1 Fits to data base prior to BaBar 2021

As a first step, we update the combined fit presented in Ref. [14], to reflect several recent developments and provide a first demonstration of the consequences of the IB corrections included in the new fit function. Regarding the data base, the SND data set [131] has been superseded by the update from Ref. [132], and likewise Ref. [133] has been superseded by Ref. [86], which we will consider in Sec. 5.2. All other data sets from SND [134–136] and CMD-2 [137–140] are treated as described in Ref. [14], while the old data from DM1 [141], DM2 [142], and ND [143] are no longer included. The motivation for this cut is given by inconsistencies that exist especially in the energy range between the ω and ϕ resonances compared to the modern data sets. Previously, these tensions in the data base essentially resulted in a slightly worse χ^2/dof , but, as expected, the size of the ρ - ω mixing contribution depends more strongly on the line shape between the resonances, in such a way that such inconsistencies can no longer be tolerated without distorting the ρ - ω mixing signal. We also update the resonance parameters of the excited ω states [117]

$$\begin{aligned} M_{\omega'} &= 1410(60) \text{ MeV}, & \Gamma_{\omega'} &= 290(190) \text{ MeV}, \\ M_{\omega''} &= 1670(30) \text{ MeV}, & \Gamma_{\omega''} &= 315(35) \text{ MeV}. \end{aligned} \quad (5.1)$$

However, given that the ω' parameters are rather uncertain, we also considered variants in which $M_{\omega'}$, $\Gamma_{\omega'}$ are allowed to vary, revealing in some cases a relevant sensitivity to $M_{\omega'}$, which will therefore be added as a free parameter. A D'Agostini bias [144] from correlated systematic errors is avoided by an iterative procedure [145], see Ref. [14] for more details.

The new fit function decomposes as follows: the normalization $a(q^2)$ is parameterized as in Eq. (2.8), with the ω contribution multiplied by $g_\pi(q^2)$ defined as in Eq. (4.7). Furthermore, all data sets are assumed to contain FSR corrections, which we remove using $\eta_{3\pi}(q^2)$ prior to the fit. Only in the final step, the calculation of the HVP loop integral (4.8), are the FSR corrections added back. This procedure follows the same approach as for $e^+e^- \rightarrow \pi^+\pi^-$, since the dispersive representation, strictly speaking, only applies for the amplitudes from which virtual-photon corrections have been removed.

The results for this updated fit are shown in Table 1. First of all, we observe a clear improvement of the χ^2/dof when including ρ - ω mixing, from about 1.4 to 1.2, which is reflected by the fact that all fits prefer a non-zero value of $\text{Re } \epsilon_\omega$ at high significance (about 5σ in terms of the fit uncertainty). Remarkably, the resulting value of $\text{Re } \epsilon_\omega$ comes out largely consistent with the extraction from $e^+e^- \rightarrow \pi^+\pi^-$, $\text{Re } \epsilon_\omega = 1.97(3) \times 10^{-3}$ [81]. Moreover, since the fits are still not perfect, suggesting residual systematic tensions in the

p_{conf}	$n_{\text{conf}} = 0$			$n_{\text{conf}} = 1$		
	2	3	4	2	3	4
χ^2/dof	274.4/228	271.2/227	270.4/226	287.5/228	284.5/227	271.6/226
	= 1.21	= 1.19	= 1.20	= 1.26	= 1.25	= 1.20
p -value	0.02	0.02	0.02	0.005	0.006	0.02
M_ω [MeV]	782.70(3)	782.69(3)	782.70(3)	782.70(3)	782.70(3)	782.69(3)
Γ_ω [MeV]	8.73(3)	8.74(3)	8.74(4)	8.73(3)	8.73(3)	8.71(4)
M_ϕ [MeV]	1019.20(1)	1019.19(1)	1019.19(1)	1019.20(1)	1019.20(1)	1019.21(1)
Γ_ϕ [MeV]	4.25(3)	4.24(3)	4.24(3)	4.25(3)	4.25(3)	4.26(3)
$M_{\omega'}$ [GeV]	1.433(17)	1.416(24)	1.408(22)	1.383(11)	1.392(10)	1.425(29)
c_ω [GeV $^{-1}$]	2.91(2)	2.92(2)	2.93(3)	2.93(2)	2.92(2)	2.88(3)
c_ϕ [GeV $^{-1}$]	-0.388(3)	-0.388(3)	-0.387(3)	-0.388(3)	-0.388(3)	-0.390(3)
$c_{\omega'}$ [GeV $^{-1}$]	-0.22(4)	-0.12(6)	-0.15(7)	-0.23(5)	-0.29(7)	0.13(7)
$c_{\omega''}$ [GeV $^{-1}$]	-1.64(7)	-1.54(8)	-1.51(10)	-0.89(6)	-0.93(7)	3.37(7)
c_1 [GeV $^{-3}$]	-0.34(8)	-0.25(9)	-0.16(14)	-1.31(9)	-1.30(9)	-2.14(6)
c_2 [GeV $^{-3}$]	-1.26(5)	-1.34(7)	-1.40(10)	-0.29(10)	-0.32(10)	-1.81(5)
c_3 [GeV $^{-3}$]	—	-0.53(7)	-0.50(8)	—	-0.23(8)	-0.62(6)
c_4 [GeV $^{-3}$]	—	—	1.38(9)	—	—	2.80(12)
$10^4 \times \xi_{\text{CMD-2}}$	1.3(5)	1.2(5)	1.2(5)	1.3(5)	1.3(5)	1.3(5)
$10^3 \times \text{Re } \epsilon_\omega$	1.48(28)	1.42(28)	1.46(28)	1.62(28)	1.61(29)	1.39(30)
$10^{10} \times a_\mu^{3\pi} _{\leq 1.8 \text{ GeV}}$	45.68(48)	45.84(49)	46.01(54)	45.83(51)	45.77(51)	45.18(51)
$10^{10} \times a_\mu^{\text{FSR}}[3\pi]$	0.51(1)	0.51(1)	0.51(1)	0.51(1)	0.51(1)	0.50(1)
$10^{10} \times a_\mu^{\rho-\omega}[3\pi]$	-2.62(49)	-2.54(49)	-2.61(49)	-2.95(50)	-2.91(51)	-2.32(49)

Table 1. Fits to the combination of SND [132, 134–136] and CMD-2' [137–140] (the prime indicates the data selection as detailed in Ref. [14], including the energy calibration $\xi_{\text{CMD-2}}$). p_{conf} denotes the number of degrees of freedom in the conformal polynomial $C_p(q^2)$, n_{conf} refers to the asymptotic behavior $\text{Im } C_p(q^2) \sim q^{-(2n_{\text{conf}}+1)}$. All couplings are given in units of $1/e = 1/\sqrt{4\pi\alpha}$, in accordance with Ref. [14]. The uncertainties refer to fit errors only, they are not yet rescaled by $S = \sqrt{\chi^2/\text{dof}}$.

data base, we will inflate the final errors by a scale factor $S = \sqrt{\chi^2/\text{dof}}$. Table 1 also includes the entire HVP integral $a_\mu^{3\pi}$, the FSR contribution a_μ^{FSR} , and the ρ - ω mixing contribution $a_\mu^{\rho-\omega}$, all integrated up to 1.8 GeV. To isolate first-order IB effects, we follow Ref. [81] and define a_μ^{FSR} for $\epsilon_\omega = 0$ and $a_\mu^{\rho-\omega}$ with FSR corrections switched off. A more detailed account of the consequences for IB effects in a_μ will be given in Sec. 6, but one can already anticipate that $a_\mu^{\rho-\omega}$ comes out large and negative, leading to a significant cancellation with $a_\mu^{\rho-\omega}[2\pi] = 3.68(17) \times 10^{-10}$ [81].

To understand how robust this cancellation is, it is critical to study the systematic uncertainties in $a_\mu^{\rho-\omega}[3\pi]$. As argued in Sec. 4, the main effect is expected from the assumptions on the line shape, which we determined in such a way that analyticity and unitarity constraints from the coupled-channel system are incorporated, in order to ensure consis-

p_{conf}	$\delta_\epsilon = 3.5^\circ$			$\delta_\epsilon \text{ free}$		
	2	3	4	2	3	4
χ^2/dof	276.4/228	271.4/227	269.9/226	275.0/227	271.2/226	269.8/225
	= 1.21	= 1.20	= 1.19	= 1.21	= 1.20	= 1.20
p -value	0.02	0.02	0.02	0.02	0.02	0.02
M_ω [MeV]	782.69(3)	782.69(3)	782.70(3)	782.70(3)	782.69(3)	782.70(3)
Γ_ω [MeV]	8.71(3)	8.73(3)	8.74(4)	8.74(4)	8.74(4)	8.73(3)
M_ϕ [MeV]	1019.20(1)	1019.19(1)	1019.20(1)	1019.20(1)	1019.19(1)	1019.20(2)
Γ_ϕ [MeV]	4.25(3)	4.24(3)	4.24(3)	4.25(3)	4.24(3)	4.24(3)
$M_{\omega'}$ [GeV]	1.432(16)	1.415(24)	1.405(19)	1.433(17)	1.416(24)	1.403(19)
c_ω [GeV $^{-1}$]	2.92(2)	2.93(2)	2.95(3)	2.90(3)	2.92(3)	2.95(4)
c_ϕ [GeV $^{-1}$]	-0.389(3)	-0.388(3)	-0.387(3)	-0.388(3)	-0.388(3)	-0.387(3)
$c_{\omega'}$ [GeV $^{-1}$]	-0.22(4)	-0.12(6)	-0.16(7)	-0.22(4)	-0.12(6)	-0.16(7)
$c_{\omega''}$ [GeV $^{-1}$]	-1.65(6)	-1.55(8)	-1.51(9)	-1.63(7)	-1.54(8)	-1.50(9)
c_1 [GeV $^{-3}$]	-0.33(8)	-0.24(9)	-0.12(15)	-0.34(8)	-0.25(10)	-0.09(18)
c_2 [GeV $^{-3}$]	-1.26(5)	-1.34(7)	-1.43(10)	-1.26(5)	-1.34(7)	-1.45(12)
c_3 [GeV $^{-3}$]	—	-0.54(7)	-0.50(8)	—	-0.53(7)	-0.49(8)
c_4 [GeV $^{-3}$]	—	—	1.40(9)	—	—	1.42(10)
$10^4 \times \xi_{\text{CMD-2}}$	1.3(5)	1.2(5)	1.3(5)	1.3(5)	1.2(5)	1.3(5)
$10^3 \times \text{Re } \epsilon_\omega$	1.49(29)	1.45(29)	1.51(29)	1.43(29)	1.43(29)	1.54(30)
δ_ϵ [°]	3.5	3.5	3.5	-4.2(7.1)	0.5(7.2)	5.4(7.5)
$10^{10} \times a_\mu^{3\pi} _{\leq 1.8 \text{ GeV}}$	45.56(48)	45.73(49)	45.95(53)	45.82(49)	45.82(50)	45.94(57)
$10^{10} \times a_\mu^{\text{FSR}}[3\pi]$	0.51(1)	0.51(1)	0.51(1)	0.50(1)	0.51(1)	0.52(1)
$10^{10} \times a_\mu^{\rho-\omega}[3\pi]$	-2.99(58)	-2.92(58)	-3.08(58)	-2.13(93)	-2.59(95)	-3.33(1.17)

Table 2. Same as Table 1 ($n_{\text{conf}} = 0$), with $\delta_\epsilon = 3.5^\circ$ (left) and a free fit parameter (right).

tency with the 2π contribution. Beyond such considerations, the analysis from Ref. [81] demonstrates that in the 2π case the biggest impact on the line shape arises from the small IB phase δ_ϵ in ϵ_ω , generated by $\pi^0\gamma$ and other radiative channels. To quantify its impact, we consider three scenarios: (i) $\delta_\epsilon = 0$ (as assumed in Table 1), (ii) $\delta_\epsilon = 3.5^\circ$ (as expected from narrow-resonance arguments [81]), and (iii) a free phase δ_ϵ as additional fit parameter. To avoid unphysical imaginary parts below threshold, we implement this phase via

$$\epsilon_\omega \rightarrow \text{Re } \epsilon_\omega + i\text{Im } \epsilon_\omega \frac{\left(1 - \frac{M_{\pi^0}^2}{q^2}\right)^3}{\left(1 - \frac{M_{\pi^0}^2}{M_\omega^2}\right)^3} \theta(q^2 - M_{\pi^0}^2), \quad (5.2)$$

motivated by the main decay channel $\rho \rightarrow \pi^0\gamma \rightarrow \omega$ that can generate such a phase. The results for (ii) and (iii) collected in Table 2 show that the data are not sensitive to δ_ϵ , but the variation in $a_\mu^{\rho-\omega}$ provides some indication for the uncertainty associated with the

p_{conf}	$n_{\text{conf}} = 0$			$n_{\text{conf}} = 1$		
	2	3	4	2	3	4
χ^2/dof	183.7/130	183.7/129	181.7/128	219.7/130	216.7/129	214.7/128
	= 1.41	= 1.42	= 1.42	= 1.69	= 1.68	= 1.68
p -value	0.001	0.001	0.001	1×10^{-6}	2×10^{-6}	2×10^{-6}
M_ω [MeV]	782.54(1)	782.54(1)	782.54(1)	782.54(1)	782.54(1)	782.54(1)
Γ_ω [MeV]	8.72(2)	8.72(2)	8.72(2)	8.70(2)	8.69(2)	8.69(2)
M_ϕ [MeV]	1019.28(1)	1019.28(1)	1019.28(1)	1019.28(1)	1019.28(1)	1019.28(1)
Γ_ϕ [MeV]	4.29(1)	4.29(1)	4.29(1)	4.29(1)	4.29(1)	4.29(1)
$M_{\omega'}$ [GeV]	1.457(8)	1.456(9)	1.471(9)	1.394(5)	1.400(6)	1.411(9)
c_ω [GeV $^{-1}$]	2.96(2)	2.96(2)	2.95(2)	2.94(2)	2.94(2)	2.93(3)
c_ϕ [GeV $^{-1}$]	-0.380(2)	-0.380(3)	-0.379(2)	-0.378(2)	-0.378(2)	-0.378(2)
$c_{\omega'}$ [GeV $^{-1}$]	-0.37(5)	-0.37(8)	-0.48(10)	-0.46(6)	-0.51(7)	-0.53(7)
$c_{\omega''}$ [GeV $^{-1}$]	-2.04(7)	-2.03(14)	-2.44(26)	-1.11(5)	-1.16(5)	-1.25(8)
c_1 [GeV $^{-3}$]	0.24(11)	0.23(13)	0.29(11)	-1.11(6)	-1.06(6)	-1.07(6)
c_2 [GeV $^{-3}$]	-1.15(4)	-1.16(7)	-0.76(25)	-0.16(7)	-0.14(6)	-0.09(8)
c_3 [GeV $^{-3}$]	—	-1.01(15)	-1.45(27)	—	-0.33(7)	-0.31(7)
c_4 [GeV $^{-3}$]	—	—	1.17(12)	—	—	-0.09(8)
$10^3 \times \text{Re } \epsilon_\omega$	1.73(22)	1.73(22)	1.70(22)	1.85(23)	1.83(23)	1.79(24)
$10^{10} \times a_\mu^{3\pi} _{\leq 1.8 \text{ GeV}}$	45.98(44)	45.99(44)	45.84(46)	45.78(44)	45.81(42)	45.74(44)
$10^{10} \times a_\mu^{\text{FSR}}[3\pi]$	0.51(1)	0.51(1)	0.51(1)	0.51(1)	0.51(1)	0.50(1)
$10^{10} \times a_\mu^{\rho-\omega}[3\pi]$	-3.09(38)	-3.09(38)	-3.02(38)	-3.33(41)	-3.31(41)	-3.24(42)

Table 3. Same as Table 1, but for the BaBar 2021 data set [86].

assumed line shape.

5.2 Fits to BaBar 2021

Next, we perform the same fits as in Sec. 5.1 to the BaBar data [86]. This data set is split into two parts, above and below $\sqrt{q^2} = 1.1$ GeV. For the data set below 1.1 GeV, we use the statistical and systematic covariance matrices as provided in Ref. [86], for the data set above 1.1 GeV we assume the systematic errors to be 100% correlated. In either case we use the bare cross sections as provided, again interpreted as including soft FSR effects.

In addition to the iterative procedure required to obtain unbiased fit results, another complication for data taken using initial-state radiation (ISR) concerns the energy calibration. In contrast to the energy-scan experiments SND or CMD-2, the cross-section data do not correspond to a set beam energy, but are provided in bins, with events distributed in accordance with the underlying cross section. Accordingly, the actual observable for a bin

p_{conf}	$\delta_\epsilon = 3.5^\circ$			$\delta_\epsilon \text{ free}$		
	2	3	4	2	3	4
χ^2/dof	179.7/130	179.6/129	178.1/128	176.3/129	174.3/128	174.1/127
	= 1.38	= 1.39	= 1.39	= 1.37	= 1.36	= 1.37
p -value	0.003	0.002	0.002	0.004	0.004	0.004
M_ω [MeV]	782.54(1)	782.54(1)	782.54(1)	782.54(1)	782.54(1)	782.54(1)
Γ_ω [MeV]	8.71(2)	8.71(2)	8.71(2)	8.71(2)	8.70(2)	8.70(2)
M_ϕ [MeV]	1019.28(1)	1019.28(1)	1019.28(1)	1019.28(1)	1019.28(1)	1019.28(1)
Γ_ϕ [MeV]	4.29(1)	4.29(1)	4.29(1)	4.29(1)	4.29(1)	4.29(1)
$M_{\omega'}$ [GeV]	1.457(2)	1.454(12)	1.466(10)	1.454(9)	1.443(9)	1.448(17)
c_ω [GeV $^{-1}$]	2.98(2)	2.98(2)	2.97(2)	3.01(3)	3.03(3)	3.02(3)
c_ϕ [GeV $^{-1}$]	-0.380(2)	-0.380(2)	-0.379(2)	-0.379(2)	-0.379(2)	-0.379(2)
$c_{\omega'}$ [GeV $^{-1}$]	-0.40(4)	-0.37(8)	-0.45(10)	-0.44(6)	-0.37(7)	-0.38(8)
$c_{\omega''}$ [GeV $^{-1}$]	-2.14(7)	-2.08(14)	-2.40(24)	-2.30(10)	-2.18(13)	-2.27(21)
c_1 [GeV $^{-3}$]	0.36(10)	0.32(13)	0.35(11)	0.57(14)	0.55(14)	0.53(14)
c_2 [GeV $^{-3}$]	-1.13(3)	-1.15(7)	-0.84(23)	-1.08(5)	-1.15(7)	-1.06(21)
c_3 [GeV $^{-3}$]	—	-1.06(16)	-1.39(25)	—	-1.13(13)	-1.21(23)
c_4 [GeV $^{-3}$]	—	—	1.25(11)	—	—	1.45(11)
$10^3 \times \text{Re } \epsilon_\omega$	1.84(22)	1.84(22)	1.81(23)	1.93(23)	1.96(22)	1.95(23)
δ_ϵ [°]	3.5	3.5	3.5	9.8(3.1)	12.2(3.2)	11.9(3.5)
$10^{10} \times a_\mu^{3\pi} _{\leq 1.8 \text{ GeV}}$	45.92(43)	45.95(45)	45.82(45)	45.77(44)	45.82(45)	45.79(49)
$10^{10} \times a_\mu^{\text{FSR}}[3\pi]$	0.52(1)	0.52(1)	0.52(1)	0.53(1)	0.54(1)	0.54(1)
$10^{10} \times a_\mu^{\rho-\omega}[3\pi]$	-3.75(45)	-3.75(45)	-3.67(45)	-4.83(72)	-5.31(72)	-5.20(82)

Table 4. Same as Table 2, but for the BaBar 2021 data set [86].

$[q_{i,\text{min}}^2, q_{i,\text{max}}^2]$ is given by

$$f(x_i) = \frac{1}{q_{i,\text{max}}^2 - q_{i,\text{min}}^2} \int_{q_{i,\text{min}}^2}^{q_{i,\text{max}}^2} dq^2 \sigma_{e^+e^- \rightarrow 3\pi(\gamma)}(q^2), \quad (5.3)$$

or, equivalently, the actual q_i^2 , replacing the center of the bin, can be obtained by solving $f(x_i) = \sigma_{e^+e^- \rightarrow 3\pi(\gamma)}(q_i^2)$. The results of the fits are summarized in Tables 3 and 4. In general, the conclusions regarding ρ - ω mixing are similar as for the previous fits in Sec. 5.1. While there is some indication that a positive phase is favored, the gain in the χ^2 is marginal, and we conclude that also in this case the data are hardly sensitive to δ_ϵ . The real part $\text{Re } \epsilon_\omega$ comes out slightly larger, but, within uncertainties, in agreement with the direct-scan experiments. More problematic is the discrepancy in the pole parameters of ω and ϕ , with M_ω significantly below the values extracted from the direct-scan experiments, and M_ϕ significantly above.

p_{conf}	$n_{\text{conf}} = 0$			$n_{\text{conf}} = 1$		
	2	3	4	2	3	4
χ^2/dof	504.9/368	494.7/367	481.9/366	545.9/368	537.8/367	537.3/366
	= 1.37	= 1.35	= 1.32	= 1.48	= 1.47	= 1.47
p -value	3×10^{-6}	1×10^{-5}	4×10^{-5}	4×10^{-9}	1×10^{-8}	1×10^{-8}
M_ω [MeV]	782.70(3)	782.70(3)	782.70(3)	782.71(3)	782.70(3)	782.70(3)
Γ_ω [MeV]	8.70(2)	8.71(2)	8.72(2)	8.71(2)	8.70(2)	8.70(2)
M_ϕ [MeV]	1019.21(1)	1019.21(1)	1019.21(1)	1019.22(1)	1019.22(1)	1019.22(1)
Γ_ϕ [MeV]	4.27(1)	4.27(1)	4.27(1)	4.27(1)	4.27(1)	4.27(1)
$M_{\omega'}$ [GeV]	1.445(10)	1.436(23)	1.418(11)	1.395(6)	1.403(6)	1.408(9)
c_ω [GeV $^{-1}$]	2.93(1)	2.93(1)	2.96(2)	2.95(1)	2.94(1)	2.94(2)
c_ϕ [GeV $^{-1}$]	-0.380(1)	-0.380(1)	-0.381(2)	-0.381(1)	-0.381(1)	-0.381(1)
$c_{\omega'}$ [GeV $^{-1}$]	-0.24(3)	-0.15(4)	-0.23(5)	-0.29(3)	-0.38(4)	-0.37(5)
$c_{\omega''}$ [GeV $^{-1}$]	-1.77(4)	-1.67(5)	-1.59(6)	-1.02(4)	-1.09(4)	-1.13(7)
c_1 [GeV $^{-3}$]	-0.18(5)	-0.13(6)	0.03(8)	-1.16(5)	-1.11(5)	-1.11(5)
c_2 [GeV $^{-3}$]	-1.21(3)	-1.29(4)	-1.43(6)	-0.16(5)	-0.16(4)	-0.15(5)
c_3 [GeV $^{-3}$]	—	-0.65(5)	-0.57(6)	—	-0.41(5)	-0.40(5)
c_4 [GeV $^{-3}$]	—	—	1.35(5)	—	—	-0.03(5)
$10^4 \times \xi_{\text{CMD-2}}$	1.4(5)	1.3(5)	1.3(5)	1.4(5)	1.4(5)	1.4(5)
$10^3 \times \xi_{\text{BaBar}}$	1.3(2)	1.3(2)	1.3(2)	1.3(2)	1.3(2)	1.3(2)
$10^3 \times \xi'_{\text{BaBar}}$ [GeV $^{-1}$]	-2.3(3)	-2.3(4)	-2.3(3)	-2.3(4)	-2.3(4)	-2.3(4)
$10^3 \times \text{Re } \epsilon_\omega$	1.51(18)	1.49(18)	1.60(17)	1.71(18)	1.68(17)	1.65(19)
$10^{10} \times a_\mu^{3\pi} _{\leq 1.8 \text{ GeV}}$	45.74(31)	45.91(32)	46.26(33)	45.96(31)	45.92(31)	45.86(32)
$10^{10} \times a_\mu^{\text{FSR}}[3\pi]$	0.51(0)	0.51(0)	0.52(0)	0.51(0)	0.51(0)	0.51(0)
$10^{10} \times a_\mu^{\rho-\omega}[3\pi]$	-2.70(31)	-2.68(31)	-2.91(30)	-3.14(31)	-3.08(30)	-3.03(33)

Table 5. Same as Table 1, but for the global fit to SND [132, 134–136], CMD-2' [137–140], and BaBar [86].

5.3 Global fit

From the fits presented in Secs. 5.1 and 5.2 it is clear that some tensions in the data base are present that will prevent a global fit of acceptable fit quality, in fact, already the fits to the BaBar data [86] alone display rather low p -values. In the end, we will attempt to remedy this shortcoming by introducing scale factors $S = \sqrt{\chi^2/\text{dof}}$ to try and include unaccounted-for systematic effects. More critical than the overall fit quality is the mismatch in M_ω and M_ϕ into opposite directions, which cannot be resolved via a linear shift in the energy calibration, as was included in Ref. [14] for part of the CMD-2 data [140] and vital for a global analysis of $e^+e^- \rightarrow \pi^+\pi^-$ [13, 81]. However, a consistent energy calibration of ISR data covering both the ω and ϕ resonances is challenging, as reflected by the additional uncertainties

p_{conf}	$\delta_\epsilon = 3.5^\circ$			$\delta_\epsilon \text{ free}$		
	2	3	4	2	3	4
χ^2/dof	512.7/368	497.2/367	479.4/366	498.4/367	494.1/366	478.3/365
	= 1.39	= 1.35	= 1.31	= 1.36	= 1.35	= 1.31
$p\text{-value}$	8×10^{-7}	7×10^{-6}	6×10^{-5}	6×10^{-6}	9×10^{-6}	6×10^{-5}
M_ω [MeV]	782.69(2)	782.70(3)	782.70(2)	782.70(3)	782.70(2)	782.70(2)
Γ_ω [MeV]	8.69(2)	8.70(2)	8.72(2)	8.72(2)	8.71(2)	8.71(2)
M_ϕ [MeV]	1019.22(1)	1019.21(1)	1019.21(1)	1019.21(1)	1019.21(1)	1019.22(1)
Γ_ϕ [MeV]	4.27(1)	4.27(1)	4.27(1)	4.27(1)	4.27(1)	4.27(1)
$M_{\omega'}$ [GeV]	1.444(9)	1.432(5)	1.412(10)	1.445(10)	1.437(3)	1.407(6)
c_ω [GeV $^{-1}$]	2.93(1)	2.94(2)	2.97(2)	2.91(2)	2.93(2)	2.99(1)
c_ϕ [GeV $^{-1}$]	-0.380(1)	-0.380(1)	-0.382(1)	-0.381(1)	-0.380(1)	-0.381(1)
$c_{\omega'}$ [GeV $^{-1}$]	-0.25(3)	-0.13(4)	-0.23(5)	-0.23(3)	-0.16(4)	-0.24(2)
$c_{\omega''}$ [GeV $^{-1}$]	-1.79(4)	-1.68(5)	-1.59(6)	-1.72(5)	-1.67(5)	-1.58(1)
c_1 [GeV $^{-3}$]	-0.15(5)	-0.10(5)	0.11(8)	-0.22(6)	-0.15(6)	0.19(4)
c_2 [GeV $^{-3}$]	-1.20(3)	-1.30(4)	-1.48(5)	-1.22(3)	-1.28(4)	-1.51(3)
c_3 [GeV $^{-3}$]	—	-0.65(4)	-0.56(5)	—	-0.65(5)	-0.55(1)
c_4 [GeV $^{-3}$]	—	—	1.40(5)	—	—	1.44(2)
$10^4 \times \xi_{\text{CMD-2}}$	1.4(5)	1.3(5)	1.3(5)	1.3(5)	1.2(5)	1.3(5)
$10^3 \times \xi_{\text{BaBar}}$	1.3(2)	1.3(2)	1.3(2)	1.3(2)	1.3(2)	1.3(2)
$10^3 \times \xi'_{\text{BaBar}}$ [GeV $^{-1}$]	-2.3(3)	-2.3(4)	-2.3(3)	-2.3(3)	-2.3(3)	-2.3(3)
$10^3 \times \text{Re } \epsilon_\omega$	1.45(18)	1.49(18)	1.68(17)	1.44(18)	1.47(17)	1.72(10)
δ_ϵ [°]	3.5	3.5	3.5	-7.2(3.3)	-2.2(3.6)	6.8(1.8)
$10^{10} \times a_\mu^{3\pi} _{\leq 1.8 \text{ GeV}}$	45.61(30)	45.81(31)	46.22(32)	46.00(31)	45.97(32)	46.17(26)
$10^{10} \times a_\mu^{\text{FSR}}[3\pi]$	0.51(0)	0.51(0)	0.52(0)	0.50(0)	0.51(0)	0.53(0)
$10^{10} \times a_\mu^{\rho-\omega}[3\pi]$	-2.93(36)	-3.04(37)	-3.47(34)	-1.87(46)	-2.42(51)	-3.97(34)

Table 6. Same as Table 2, but for the global fit to SND [132, 134–136], CMD-2' [137–140], and BaBar [86].

$\Delta M_\omega = 0.06 \text{ MeV}$ and $\Delta M_\phi = 0.08 \text{ MeV}$ quoted in Ref. [86].⁵ We emphasize that the agreement with PDG parameters found in Ref. [86] is accidental, relying on including the ω mass determination from $\bar{p}p \rightarrow \omega\pi^0\pi^0$ [146] in the average despite being in conflict with $e^+e^- \rightarrow 3\pi$, but acknowledge that the associated uncertainties make it appear likely that the energy calibration in the direct-scan data should be considered more robust. To account for the tensions in M_ω and M_ϕ in a minimal fashion, we thus allow for a quadratic energy rescaling

$$\sqrt{s} \rightarrow \sqrt{s} + \xi(\sqrt{s} - 3M_\pi) + \xi'(\sqrt{s} - 3M_\pi)^2 \quad (5.4)$$

⁵We thank M. Davier and V. Druzhinin for their assessment of the expected accuracy of the energy calibration in the ISR data.

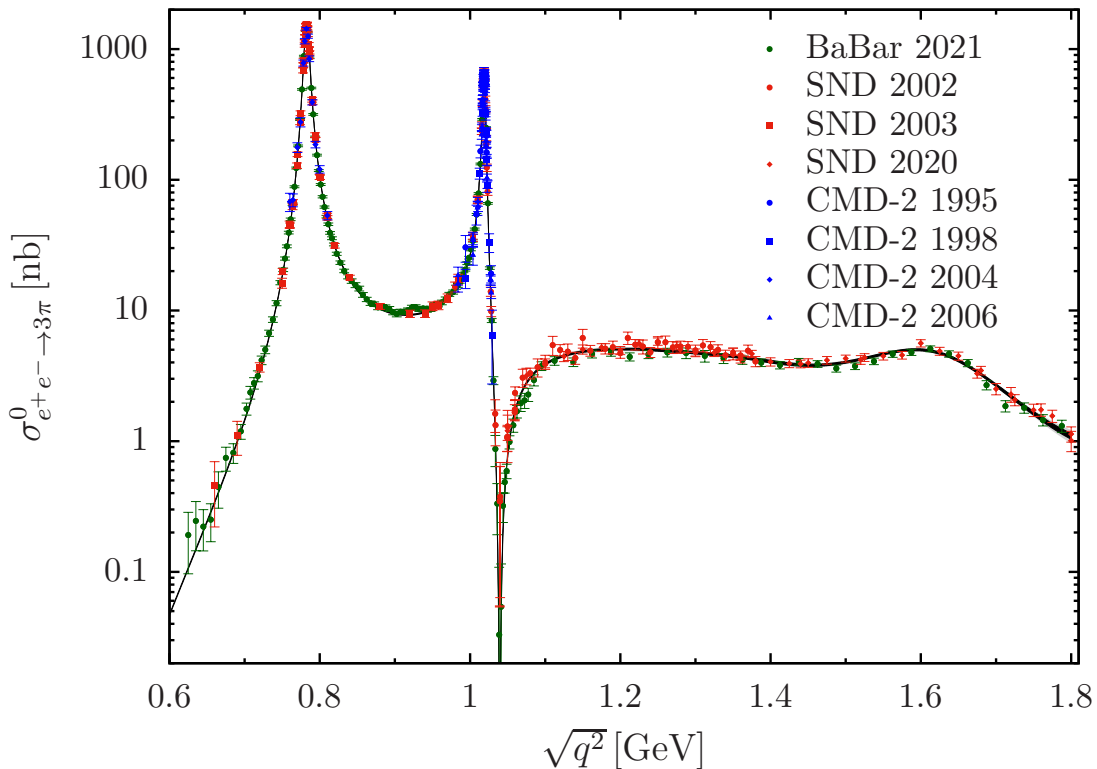


Figure 3. Fit to the bare $e^+e^- \rightarrow 3\pi$ data sets as detailed in Sec. 5.1. The gray band shows the total uncertainty, while the black band represents the fit uncertainty only. The difference between the two is hardly visible on the logarithmic plot, as they are of similar size in most regions.

in the fit to Ref. [86].⁶ The results of this global fit are summarized in Tables 5 and 6. In particular, the comparison of the fits with $\delta_\epsilon = 0$, $\delta_\epsilon = 3.5^\circ$, and a free δ_ϵ again shows that the sensitivity to this parameter is small, with marginal changes in the fit quality. In contrast, fits with improved asymptotic behavior, $n_{\text{conf}} = 1$, do display a significantly worse χ^2/dof .

To assign uncertainties to our results we thus proceed as follows. First, the statistical errors are inflated by the scale factor $S = \sqrt{\chi^2/\text{dof}}$. Following Ref. [14], we take the fits with $p_{\text{conf}} = 3$ to define the central values, as several fits with $p_{\text{conf}} = 4$ already display signs of overfitting. The systematic error from the truncation of the conformal polynomial is then estimated as the maximum difference compared to the fit variants with $p_{\text{conf}} = 2, 4$. In addition, in Ref. [14] we included the variation to fits with $n_{\text{conf}} = 1$, but given the observations above this recipe no longer appears appropriate with our improved dispersive formalism. The remaining uncertainties are better represented by scanning over the sensitivity to δ_ϵ , given that these fits are not distinguished by the χ^2 criterion. In view of the narrow-width arguments in favor of a small phase $\delta_\epsilon = 3.5(1.0)^\circ$ [81], combined with

⁶We apply this rescaling only to the data set below 1.1 GeV, since no tensions arise in the fit of the data above.

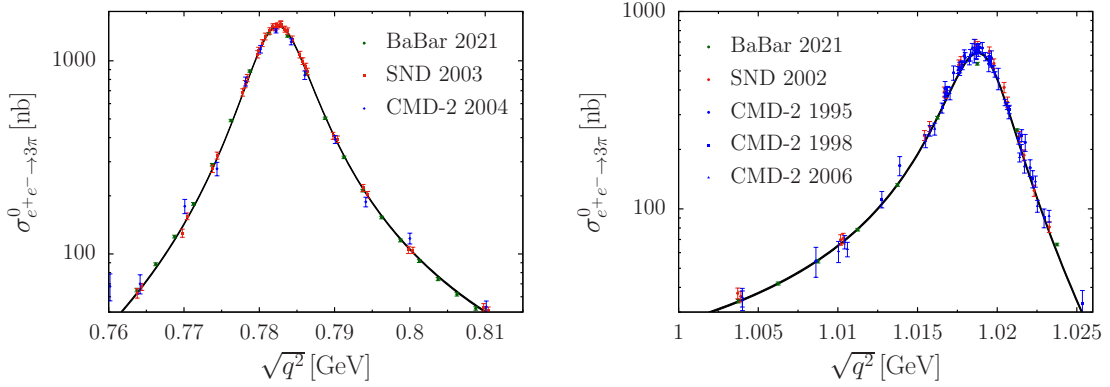


Figure 4. Same as Fig. 3, but for the close-up views of the ω and ϕ resonance regions.

the lack of sensitivity to this phase in the $e^+e^- \rightarrow 3\pi$ data themselves, we quote the results at $\delta_\epsilon = 0$ as central values, while assigning the change to $\delta_\epsilon = 3.5^\circ$ as an additional source of systematic uncertainty. Our central fit is illustrated in Fig. 3, with zoom-in views of the ω and ϕ regions in Fig. 4.

With this procedure, we find

$$\begin{aligned}
 M_\omega &= 782.697(32)(4)(4)[32] \text{ MeV}, & \Gamma_\omega &= 8.711(21)(12)(10)[26] \text{ MeV}, \\
 M_\phi &= 1019.211(17)(4)(1)[17] \text{ MeV}, & \Gamma_\phi &= 4.270(13)(3)(1)[13] \text{ MeV}, \\
 M_{\omega'} &= 1436(26)(17)(6)[32] \text{ MeV}, \\
 \text{Re } \epsilon_\omega &= 1.49(21)(11)(8)[25] \times 10^{-3}, & & (5.5)
 \end{aligned}$$

where the errors refer to statistics, truncation of the conformal polynomial, dependence on δ_ϵ , and quadratic sum, respectively. The mass of the ω' comes out in agreement with Eq. (5.1), the mixing parameter about 1.9σ below the expectation from $e^+e^- \rightarrow 2\pi$. The comparison of the ω and ϕ resonance parameters to our previous determinations [14, 17, 82] as well as the PDG values [117] is given in Table 7. For the mass parameters, the main change concerns the improved functional form of the representation including ρ - ω interference, which leads to an increase in M_ω of 0.06 MeV, while the change in M_ϕ is much smaller. In both cases, the precision hardly changes when including the BaBar data [86], ultimately due to the necessity of the energy rescaling (5.4). In contrast, the uncertainties in the widths decrease appreciably when including Ref. [86], about a factor 2 for Γ_ω and a factor 4 for Γ_ϕ . In the latter case, the determination from $e^+e^- \rightarrow 3\pi$ is now competitive with $e^+e^- \rightarrow \bar{K}K$, which dominates the corresponding PDG average. We find agreement with the PDG values in all cases, albeit for M_ω only due to the scale factor $S = 2.0$ included in the PDG uncertainty, reflecting the conflict between $e^+e^- \rightarrow 3\pi$ and $\bar{p}p \rightarrow \omega\pi^0\pi^0$ alluded to above. For $e^+e^- \rightarrow \pi^0\gamma$ and $e^+e^- \rightarrow \bar{K}K$ we observe mostly good agreement as well, except for M_ω in the $\pi^0\gamma$ channel, which comes out slightly lower than in 3π , and Γ_ϕ in the $\bar{K}K$ channel, in which case the 3π and $\bar{K}K$ determinations are not compatible within uncertainties.

	$e^+e^- \rightarrow \pi^0\gamma$	$e^+e^- \rightarrow \bar{K}K$	$e^+e^- \rightarrow 3\pi$		
	Ref. [17]	Ref. [82]	Ref. [14]	this work	PDG [117]
M_ω [MeV]	782.584(28)	–	782.631(28)	782.697(32)	782.53(13)
Γ_ω [MeV]	8.65(6)	–	8.71(6)	8.711(26)	8.74(13)
M_ϕ [MeV]	1019.205(55)	1019.219(4)	1019.196(21)	1019.211(17)	1019.201(16)
Γ_ϕ [MeV]	4.07(13)	4.207(8)	4.23(4)	4.270(13)	4.249(13)

Table 7. VP-subtracted resonance parameters of ω and ϕ in comparison to our previous determinations from $e^+e^- \rightarrow 3\pi$ [14], $e^+e^- \rightarrow \pi^0\gamma$ [17], and $e^+e^- \rightarrow \bar{K}K$ [82]. The last column gives the PDG values [117], with VP removed using the corrections from Ref. [46].

6 Consequences for the anomalous magnetic moment of the muon

As key application, we reevaluate the 3π contribution to HVP, including the separate effects from radiative corrections and ρ - ω mixing. Defining the latter contributions as the leading term in the corresponding IB parameters e^2 and ϵ_ω , we find

$$\begin{aligned}
a_\mu^{3\pi}|_{\leq 1.8 \text{ GeV}} &= 45.91(37)(35)(13)[53] \times 10^{-10}, \\
a_\mu^{\text{FSR}}[3\pi] &= 0.509(4)(6)(6)[9] \times 10^{-10}, \\
a_\mu^{\rho-\omega}[3\pi] &= -2.68(36)(22)(56)[70] \times 10^{-10},
\end{aligned} \tag{6.1}$$

where the errors again refer to statistics, truncation of the conformal polynomial, dependence on δ_ϵ , and quadratic sum, respectively.⁷ For the total contribution, both the statistical and systematic errors have decreased by almost a factor 2 compared to $a_\mu^{3\pi}|_{\leq 1.8 \text{ GeV}} = 46.2(6)(6) \times 10^{-10}$ [14], which traces back to including the BaBar data [86] and to the improved dispersive representation constructed in this paper. Concerning the IB corrections, the FSR piece comports with the naive scaling expectation $a_\mu^{\text{FSR}}[3\pi] \simeq a_\mu^{\text{FSR}}[2\pi]a_\mu^{3\pi}/a_\mu^{2\pi} \simeq 0.4 \times 10^{-10}$, while $a_\mu^{\rho-\omega}[3\pi]$ indeed comes out large and negative, canceling a significant portion of $a_\mu^{\rho-\omega}[2\pi] = 3.68(17) \times 10^{-10}$ [81], for the reasons anticipated in Sec. 4. The sensitivity to the assumed line shape is clearly reflected by the uncertainties quoted in Eq. (6.1), as $a_\mu^{\rho-\omega}[3\pi]$ is the only quantity for which the error derived from the variation in δ_ϵ dominates. Finally, we also provide the decomposition of the total HVP integral onto the Euclidean-time windows from Ref. [56], see Table 8.

7 Conclusions

In this work, we developed the necessary formalism to describe the leading isospin-breaking effects in $e^+e^- \rightarrow 3\pi$, which originate from infrared-enhanced radiative corrections and

⁷We emphasize that the error for FSR does not include an estimate for the subleading, non-IR-enhanced terms. In the 2π case, such corrections amount to 3% [99], which would translate here to an additional uncertainty of 0.015×10^{-10} .

	$10^{10} \times a_\mu^{3\pi} _{\leq 1.8 \text{ GeV}}$	$10^{10} \times a_\mu^{\text{FSR}}[3\pi]$	$10^{10} \times a_\mu^{\rho-\omega}[3\pi]$
short-distance window	2.51(2)(1)(0)[2]	0.026(0)(0)(0)[0]	-0.13(2)(1)(3)[3]
intermediate window	18.27(15)(12)(5)[20]	0.199(2)(2)(2)[4]	-1.03(14)(9)(21)[27]
long-distance window	25.13(20)(22)(8)[31]	0.284(2)(4)(3)[6]	-1.52(20)(12)(33)[40]
total	45.91(37)(35)(13)[53]	0.509(4)(6)(6)[9]	-2.68(36)(22)(56)[70]

Table 8. Decomposition of the total 3π HVP contribution as well as the FSR and ρ - ω components onto the short-distance, intermediate, and long-distance windows from Ref. [56].

the interference of ρ and ω resonances. For the former, we made use of the fact that the dominant effects arise as a remnant of the cancellation of infrared singularities between certain virtual-photon diagrams and bremsstrahlung corrections, leading to a generalization of the standard inclusive FSR correction factor $\eta_{2\pi}(q^2)$ for $e^+e^- \rightarrow \pi^+\pi^-$, see Sec. 3 for the derivation of the resulting $\eta_{3\pi}(q^2)$. For ρ - ω mixing, we presented an implementation based on a coupled-channel system for e^+e^- , $\pi^+\pi^-$, and 3π , preserving analyticity and unitarity properties and predicting the line shape of the ρ in a way consistent with the dispersive representation of the self energies in the multichannel system. In particular, our approach allows us to make the connection with the ρ - ω mixing parameter ϵ_ω in $e^+e^- \rightarrow \pi^+\pi^-$ manifest.

Based on this improved dispersive representation of the $e^+e^- \rightarrow 3\pi$ cross section, we performed a phenomenological analysis including the latest data from the BaBar experiment. First, we observed that including ρ - ω mixing in the description markedly improves the fit quality, demonstrating that the effect is visible in the data and can be distinguished from background despite the broad nature of the ρ . For the quantitative analysis, the main uncertainty arises from the line shape of the ρ - ω mixing contribution, which, in our framework, can be estimated by investigating the dependence on a small phase of ϵ_ω , as generated by radiative decay channels. We found that ϵ_ω comes out slightly smaller than expected from $e^+e^- \rightarrow 2\pi$, yet in view of the associated uncertainties still indicating a remarkable consistency between the two channels. As a first application, we provided the resonance parameters of ω and ϕ that correspond to the global fit to the 3π data base, see Eq. (5.5) for the final results.

The main application concerns the 3π channel in the hadronic-vacuum-polarization contribution to the anomalous magnetic moment of the muon. First, with new data from BaBar and our improved dispersive representation, both the statistical and systematic uncertainties reduce by almost a factor 2, see Eq. (6.1) for the key results. Moreover, we can quantify the contribution of the $3\pi\gamma$ channel, estimated as the combined effect of the dominant infrared-enhanced radiative corrections, as well as the impact of the ρ - ω interference. While the former scales as expected from the total size of the 2π and 3π channels, the latter is large and negative, canceling a substantial part of the ρ - ω mixing contribution in the 2π channel. This cancellation can be understood in terms of narrow-width arguments,

see Sec. 4, and likely points to a general interplay between the two channels. Our results corroborate the evaluation of the 3π channel with reduced uncertainties, and provide crucial input to a phenomenological analysis of isospin-breaking effects in the hadronic-vacuum-polarization contribution to the anomalous magnetic moment of the muon [84, 147].

Acknowledgments

We thank M. Davier and V. Druzhinin for helpful communication on Ref. [86], Dominik Stamen for providing 3π KT basis functions, and Janak Prabhu for collaboration on the electromagnetic corrections in an early stage of this project. Financial support by the DFG through the funds provided to the Sino–German Collaborative Research Center TRR110 “Symmetries and the Emergence of Structure in QCD” (DFG Project-ID 196253076 – TRR 110) and the SNSF (Project No. PCEFP2_181117) is gratefully acknowledged. MH thanks the INT at the University of Washington for its hospitality and the DOE for partial support (grant No. DE-FG02-00ER41132) during a visit when part of this work was performed.

References

- [1] B. Abi *et al.* (Muon $g - 2$), *Phys. Rev. Lett.* **126**, 141801 (2021), [arXiv:2104.03281 \[hep-ex\]](#).
- [2] T. Albahri *et al.* (Muon $g - 2$), *Phys. Rev. A* **103**, 042208 (2021), [arXiv:2104.03201 \[hep-ex\]](#).
- [3] T. Albahri *et al.* (Muon $g - 2$), *Phys. Rev. Accel. Beams* **24**, 044002 (2021), [arXiv:2104.03240 \[physics.acc-ph\]](#).
- [4] T. Albahri *et al.* (Muon $g - 2$), *Phys. Rev. D* **103**, 072002 (2021), [arXiv:2104.03247 \[hep-ex\]](#).
- [5] G. W. Bennett *et al.* (Muon $g - 2$), *Phys. Rev. D* **73**, 072003 (2006), [arXiv:hep-ex/0602035](#).
- [6] T. Aoyama *et al.*, *Phys. Rept.* **887**, 1 (2020), [arXiv:2006.04822 \[hep-ph\]](#).
- [7] T. Aoyama, M. Hayakawa, T. Kinoshita, and M. Nio, *Phys. Rev. Lett.* **109**, 111808 (2012), [arXiv:1205.5370 \[hep-ph\]](#).
- [8] T. Aoyama, T. Kinoshita, and M. Nio, *Atoms* **7**, 28 (2019).
- [9] A. Czarnecki, W. J. Marciano, and A. Vainshtein, *Phys. Rev. D* **67**, 073006 (2003), [Erratum: *Phys. Rev. D* **73**, 119901 (2006)], [arXiv:hep-ph/0212229](#).
- [10] C. Gnendiger, D. Stöckinger, and H. Stöckinger-Kim, *Phys. Rev. D* **88**, 053005 (2013), [arXiv:1306.5546 \[hep-ph\]](#).
- [11] M. Davier, A. Hoecker, B. Malaescu, and Z. Zhang, *Eur. Phys. J. C* **77**, 827 (2017), [arXiv:1706.09436 \[hep-ph\]](#).
- [12] A. Keshavarzi, D. Nomura, and T. Teubner, *Phys. Rev. D* **97**, 114025 (2018), [arXiv:1802.02995 \[hep-ph\]](#).
- [13] G. Colangelo, M. Hoferichter, and P. Stoffer, *JHEP* **02**, 006 (2019), [arXiv:1810.00007 \[hep-ph\]](#).
- [14] M. Hoferichter, B.-L. Hoid, and B. Kubis, *JHEP* **08**, 137 (2019), [arXiv:1907.01556 \[hep-ph\]](#).
- [15] M. Davier, A. Hoecker, B. Malaescu, and Z. Zhang, *Eur. Phys. J. C* **80**, 241 (2020), [Erratum: *Eur. Phys. J. C* **80**, 410 (2020)], [arXiv:1908.00921 \[hep-ph\]](#).

- [16] A. Keshavarzi, D. Nomura, and T. Teubner, *Phys. Rev. D* **101**, 014029 (2020), [arXiv:1911.00367 \[hep-ph\]](#).
- [17] B.-L. Hoid, M. Hoferichter, and B. Kubis, *Eur. Phys. J. C* **80**, 988 (2020), [arXiv:2007.12696 \[hep-ph\]](#).
- [18] A. Kurz, T. Liu, P. Marquard, and M. Steinhauser, *Phys. Lett. B* **734**, 144 (2014), [arXiv:1403.6400 \[hep-ph\]](#).
- [19] K. Melnikov and A. Vainshtein, *Phys. Rev. D* **70**, 113006 (2004), [arXiv:hep-ph/0312226](#).
- [20] G. Colangelo, M. Hoferichter, M. Procura, and P. Stoffer, *JHEP* **09**, 091 (2014), [arXiv:1402.7081 \[hep-ph\]](#).
- [21] G. Colangelo, M. Hoferichter, B. Kubis, M. Procura, and P. Stoffer, *Phys. Lett. B* **738**, 6 (2014), [arXiv:1408.2517 \[hep-ph\]](#).
- [22] G. Colangelo, M. Hoferichter, M. Procura, and P. Stoffer, *JHEP* **09**, 074 (2015), [arXiv:1506.01386 \[hep-ph\]](#).
- [23] P. Masjuan and P. Sánchez-Puertas, *Phys. Rev. D* **95**, 054026 (2017), [arXiv:1701.05829 \[hep-ph\]](#).
- [24] G. Colangelo, M. Hoferichter, M. Procura, and P. Stoffer, *Phys. Rev. Lett.* **118**, 232001 (2017), [arXiv:1701.06554 \[hep-ph\]](#).
- [25] G. Colangelo, M. Hoferichter, M. Procura, and P. Stoffer, *JHEP* **04**, 161 (2017), [arXiv:1702.07347 \[hep-ph\]](#).
- [26] M. Hoferichter, B.-L. Hoid, B. Kubis, S. Leupold, and S. P. Schneider, *Phys. Rev. Lett.* **121**, 112002 (2018), [arXiv:1805.01471 \[hep-ph\]](#).
- [27] M. Hoferichter, B.-L. Hoid, B. Kubis, S. Leupold, and S. P. Schneider, *JHEP* **10**, 141 (2018), [arXiv:1808.04823 \[hep-ph\]](#).
- [28] A. Gérardin, H. B. Meyer, and A. Nyffeler, *Phys. Rev. D* **100**, 034520 (2019), [arXiv:1903.09471 \[hep-lat\]](#).
- [29] J. Bijnens, N. Hermansson-Truedsson, and A. Rodríguez-Sánchez, *Phys. Lett. B* **798**, 134994 (2019), [arXiv:1908.03331 \[hep-ph\]](#).
- [30] G. Colangelo, F. Hagelstein, M. Hoferichter, L. Laub, and P. Stoffer, *Phys. Rev. D* **101**, 051501 (2020), [arXiv:1910.11881 \[hep-ph\]](#).
- [31] G. Colangelo, F. Hagelstein, M. Hoferichter, L. Laub, and P. Stoffer, *JHEP* **03**, 101 (2020), [arXiv:1910.13432 \[hep-ph\]](#).
- [32] T. Blum, N. Christ, M. Hayakawa, T. Izubuchi, L. Jin, C. Jung, and C. Lehner (RBC, UKQCD), *Phys. Rev. Lett.* **124**, 132002 (2020), [arXiv:1911.08123 \[hep-lat\]](#).
- [33] G. Colangelo, M. Hoferichter, A. Nyffeler, M. Passera, and P. Stoffer, *Phys. Lett. B* **735**, 90 (2014), [arXiv:1403.7512 \[hep-ph\]](#).
- [34] E.-H. Chao, R. J. Hudspith, A. Gérardin, J. R. Green, H. B. Meyer, and K. Ottnad, *Eur. Phys. J. C* **81**, 651 (2021), [arXiv:2104.02632 \[hep-lat\]](#).
- [35] E.-H. Chao, R. J. Hudspith, A. Gérardin, J. R. Green, and H. B. Meyer, *Eur. Phys. J. C* **82**, 664 (2022), [arXiv:2204.08844 \[hep-lat\]](#).
- [36] T. Blum, N. Christ, M. Hayakawa, T. Izubuchi, L. Jin, C. Jung, C. Lehner, and C. Tu (RBC, UKQCD), (2023), [arXiv:2304.04423 \[hep-lat\]](#).

- [37] C. Alexandrou *et al.* (ETM), (2022), [arXiv:2212.06704 \[hep-lat\]](#).
- [38] A. Gérardin *et al.* (BMWc), (2023), [arXiv:2305.04570 \[hep-lat\]](#).
- [39] M. Hoferichter and P. Stoffer, *JHEP* **05**, 159 (2020), [arXiv:2004.06127 \[hep-ph\]](#).
- [40] J. Lüdtkke and M. Procura, *Eur. Phys. J. C* **80**, 1108 (2020), [arXiv:2006.00007 \[hep-ph\]](#).
- [41] J. Bijnens, N. Hermansson-Truedsson, L. Laub, and A. Rodríguez-Sánchez, *JHEP* **10**, 203 (2020), [arXiv:2008.13487 \[hep-ph\]](#).
- [42] J. Bijnens, N. Hermansson-Truedsson, L. Laub, and A. Rodríguez-Sánchez, *JHEP* **04**, 240 (2021), [arXiv:2101.09169 \[hep-ph\]](#).
- [43] M. Zanke, M. Hoferichter, and B. Kubis, *JHEP* **07**, 106 (2021), [arXiv:2103.09829 \[hep-ph\]](#).
- [44] I. Danilkin, M. Hoferichter, and P. Stoffer, *Phys. Lett. B* **820**, 136502 (2021), [arXiv:2105.01666 \[hep-ph\]](#).
- [45] G. Colangelo, F. Hagelstein, M. Hoferichter, L. Laub, and P. Stoffer, *Eur. Phys. J. C* **81**, 702 (2021), [arXiv:2106.13222 \[hep-ph\]](#).
- [46] S. Holz, C. Hanhart, M. Hoferichter, and B. Kubis, *Eur. Phys. J. C* **82**, 434 (2022), [Addendum: *Eur. Phys. J. C* **82**, 1159 (2022)], [arXiv:2202.05846 \[hep-ph\]](#).
- [47] J. Leutgeb, J. Mager, and A. Rebhan, *Phys. Rev. D* **107**, 054021 (2023), [arXiv:2211.16562 \[hep-ph\]](#).
- [48] J. Bijnens, N. Hermansson-Truedsson, and A. Rodríguez-Sánchez, *JHEP* **02**, 167 (2023), [arXiv:2211.17183 \[hep-ph\]](#).
- [49] J. Lüdtkke, M. Procura, and P. Stoffer, *JHEP* **04**, 125 (2023), [arXiv:2302.12264 \[hep-ph\]](#).
- [50] M. Hoferichter, B. Kubis, and M. Zanke, (2023), [arXiv:2307.14413 \[hep-ph\]](#).
- [51] J. Grange *et al.* (Muon $g - 2$), (2015), [arXiv:1501.06858 \[physics.ins-det\]](#).
- [52] G. Colangelo *et al.*, (2022), [arXiv:2203.15810 \[hep-ph\]](#).
- [53] J. Calmet, S. Narison, M. Perrottet, and E. de Rafael, *Phys. Lett. B* **61**, 283 (1976).
- [54] M. Hoferichter and T. Teubner, *Phys. Rev. Lett.* **128**, 112002 (2022), [arXiv:2112.06929 \[hep-ph\]](#).
- [55] S. Borsanyi *et al.* (BMWc), *Nature* **593**, 51 (2021), [arXiv:2002.12347 \[hep-lat\]](#).
- [56] T. Blum *et al.* (RBC, UKQCD), *Phys. Rev. Lett.* **121**, 022003 (2018), [arXiv:1801.07224 \[hep-lat\]](#).
- [57] M. Cè *et al.*, *Phys. Rev. D* **106**, 114502 (2022), [arXiv:2206.06582 \[hep-lat\]](#).
- [58] C. Alexandrou *et al.* (ETM), *Phys. Rev. D* **107**, 074506 (2023), [arXiv:2206.15084 \[hep-lat\]](#).
- [59] A. Bazavov *et al.* (Fermilab Lattice, HPQCD, MILC), *Phys. Rev. D* **107**, 114514 (2023), [arXiv:2301.08274 \[hep-lat\]](#).
- [60] T. Blum *et al.* (RBC, UKQCD), (2023), [arXiv:2301.08696 \[hep-lat\]](#).
- [61] G. Colangelo, A. X. El-Khadra, M. Hoferichter, A. Keshavarzi, C. Lehner, P. Stoffer, and T. Teubner, *Phys. Lett. B* **833**, 137313 (2022), [arXiv:2205.12963 \[hep-ph\]](#).
- [62] M. N. Achasov *et al.* (SND), *JHEP* **01**, 113 (2021), [arXiv:2004.00263 \[hep-ex\]](#).
- [63] F. V. Ignatov *et al.* (CMD-3), (2023), [arXiv:2302.08834 \[hep-ex\]](#).

- [64] R. R. Akhmetshin *et al.* (CMD-2), *Phys. Lett. B* **648**, 28 (2007), [arXiv:hep-ex/0610021](#).
- [65] M. N. Achasov *et al.* (SND), *J. Exp. Theor. Phys.* **103**, 380 (2006), [arXiv:hep-ex/0605013](#).
- [66] J. P. Lees *et al.* (BaBar), *Phys. Rev. D* **86**, 032013 (2012), [arXiv:1205.2228 \[hep-ex\]](#).
- [67] A. Anastasi *et al.* (KLOE-2), *JHEP* **03**, 173 (2018), [arXiv:1711.03085 \[hep-ex\]](#).
- [68] M. Ablikim *et al.* (BESIII), *Phys. Lett. B* **753**, 629 (2016), [Erratum: *Phys. Lett. B* **812**, 135982 (2021)], [arXiv:1507.08188 \[hep-ex\]](#).
- [69] L. Di Luzio, A. Masiero, P. Paradisi, and M. Passera, *Phys. Lett. B* **829**, 137037 (2022), [arXiv:2112.08312 \[hep-ph\]](#).
- [70] L. Darmé, G. Grilli di Cortona, and E. Nardi, *JHEP* **06**, 122 (2022), [arXiv:2112.09139 \[hep-ph\]](#).
- [71] A. Crivellin and M. Hoferichter, *Phys. Rev. D* **108**, 013005 (2023), [arXiv:2211.12516 \[hep-ph\]](#).
- [72] N. M. Coyle and C. E. M. Wagner, (2023), [arXiv:2305.02354 \[hep-ph\]](#).
- [73] M. Passera, W. J. Marciano, and A. Sirlin, *Phys. Rev. D* **78**, 013009 (2008), [arXiv:0804.1142 \[hep-ph\]](#).
- [74] A. Crivellin, M. Hoferichter, C. A. Manzari, and M. Montull, *Phys. Rev. Lett.* **125**, 091801 (2020), [arXiv:2003.04886 \[hep-ph\]](#).
- [75] A. Keshavarzi, W. J. Marciano, M. Passera, and A. Sirlin, *Phys. Rev. D* **102**, 033002 (2020), [arXiv:2006.12666 \[hep-ph\]](#).
- [76] B. Malaescu and M. Schott, *Eur. Phys. J. C* **81**, 46 (2021), [arXiv:2008.08107 \[hep-ph\]](#).
- [77] G. Colangelo, M. Hoferichter, and P. Stoffer, *Phys. Lett. B* **814**, 136073 (2021), [arXiv:2010.07943 \[hep-ph\]](#).
- [78] M. Cè *et al.*, *JHEP* **08**, 220 (2022), [arXiv:2203.08676 \[hep-lat\]](#).
- [79] G. Colangelo, M. Hoferichter, J. Monnard, and J. Ruiz de Elvira, *JHEP* **08**, 295 (2022), [arXiv:2207.03495 \[hep-ph\]](#).
- [80] G. Chanturia, *PoS Regio2021*, 030 (2022).
- [81] G. Colangelo, M. Hoferichter, B. Kubis, and P. Stoffer, *JHEP* **10**, 032 (2022), [arXiv:2208.08993 \[hep-ph\]](#).
- [82] D. Stamen, D. Hariharan, M. Hoferichter, B. Kubis, and P. Stoffer, *Eur. Phys. J. C* **82**, 432 (2022), [arXiv:2202.11106 \[hep-ph\]](#).
- [83] C. Alexandrou *et al.* (ETM), *Phys. Rev. Lett.* **130**, 241901 (2023), [arXiv:2212.08467 \[hep-lat\]](#).
- [84] M. Hoferichter, G. Colangelo, B.-L. Hoid, B. Kubis, J. Ruiz de Elvira, D. Stamen, and P. Stoffer, *PoS LATTICE2022*, 316 (2022), [arXiv:2210.11904 \[hep-ph\]](#).
- [85] C. L. James, R. Lewis, and K. Maltman, *Phys. Rev. D* **105**, 053010 (2022), [arXiv:2109.13729 \[hep-ph\]](#).
- [86] J. P. Lees *et al.* (BaBar), *Phys. Rev. D* **104**, 112003 (2021), [arXiv:2110.00520 \[hep-ex\]](#).
- [87] D. Boito, M. Golterman, K. Maltman, and S. Peris, *Phys. Rev. D* **105**, 093003 (2022), [arXiv:2203.05070 \[hep-ph\]](#).

- [88] D. Boito, M. Golterman, K. Maltman, and S. Peris, *Phys. Rev. D* **107**, 074001 (2023), [arXiv:2211.11055 \[hep-ph\]](#).
- [89] G. Benton, D. Boito, M. Golterman, A. Keshavarzi, K. Maltman, and S. Peris, (2023), [arXiv:2306.16808 \[hep-ph\]](#).
- [90] A. Hofer, J. Gluza, and F. Jegerlehner, *Eur. Phys. J. C* **24**, 51 (2002), [arXiv:hep-ph/0107154](#).
- [91] H. Czyż, A. Grzelińska, J. H. Kühn, and G. Rodrigo, *Eur. Phys. J. C* **39**, 411 (2005), [arXiv:hep-ph/0404078](#).
- [92] J. Gluza, A. Hofer, S. Jadach, and F. Jegerlehner, *Eur. Phys. J. C* **28**, 261 (2003), [arXiv:hep-ph/0212386](#).
- [93] Y. M. Bystritskiy, E. A. Kuraev, G. V. Fedotovitch, and F. V. Ignatov, *Phys. Rev. D* **72**, 114019 (2005), [arXiv:hep-ph/0505236](#).
- [94] J. Wess and B. Zumino, *Phys. Lett. B* **37**, 95 (1971).
- [95] E. Witten, *Nucl. Phys. B* **223**, 422 (1983).
- [96] L. Ametller, M. Knecht, and P. Talavera, *Phys. Rev. D* **64**, 094009 (2001), [arXiv:hep-ph/0107127](#).
- [97] A. I. Ahmedov, G. V. Fedotovitch, E. A. Kuraev, and Z. K. Silagadze, *JHEP* **09**, 008 (2002), [arXiv:hep-ph/0201157](#).
- [98] S. Bakmaev, Y. M. Bystritskiy, and E. A. Kuraev, *Phys. Rev. D* **73**, 034010 (2006), [arXiv:hep-ph/0507219](#).
- [99] B. Moussallam, *Eur. Phys. J. C* **73**, 2539 (2013), [arXiv:1305.3143 \[hep-ph\]](#).
- [100] N. N. Khuri and S. B. Treiman, *Phys. Rev.* **119**, 1115 (1960).
- [101] M. Hoferichter, B. Kubis, S. Leupold, F. Niecknig, and S. P. Schneider, *Eur. Phys. J. C* **74**, 3180 (2014), [arXiv:1410.4691 \[hep-ph\]](#).
- [102] S. L. Adler, B. W. Lee, S. B. Treiman, and A. Zee, *Phys. Rev. D* **4**, 3497 (1971).
- [103] M. V. Terent'ev, *Phys. Lett. B* **38**, 419 (1972).
- [104] R. Aviv and A. Zee, *Phys. Rev. D* **5**, 2372 (1972).
- [105] I. J. R. Aitchison and R. J. A. Golding, *J. Phys. G* **4**, 43 (1978).
- [106] F. Niecknig, B. Kubis, and S. P. Schneider, *Eur. Phys. J. C* **72**, 2014 (2012), [arXiv:1203.2501 \[hep-ph\]](#).
- [107] S. P. Schneider, B. Kubis, and F. Niecknig, *Phys. Rev. D* **86**, 054013 (2012), [arXiv:1206.3098 \[hep-ph\]](#).
- [108] M. Hoferichter, B. Kubis, and D. Sakkas, *Phys. Rev. D* **86**, 116009 (2012), [arXiv:1210.6793 \[hep-ph\]](#).
- [109] I. V. Danilkin *et al.*, *Phys. Rev. D* **91**, 094029 (2015), [arXiv:1409.7708 \[hep-ph\]](#).
- [110] M. Dax, T. Isken, and B. Kubis, *Eur. Phys. J. C* **78**, 859 (2018), [arXiv:1808.08957 \[hep-ph\]](#).
- [111] M. Jacob and G. C. Wick, *Annals Phys.* **7**, 404 (1959), [*Annals Phys.* **281**, 774 (2000)].
- [112] M. Hoferichter, B. Kubis, and M. Zanke, *Phys. Rev. D* **96**, 114016 (2017), [arXiv:1710.00824 \[hep-ph\]](#).

- [113] J. Bijnens, A. Bramon, and F. Cornet, *Phys. Lett. B* **237**, 488 (1990).
- [114] R. A. Briceño, J. J. Dudek, R. G. Edwards, C. J. Shultz, C. E. Thomas, and D. J. Wilson (HadSpec), *Phys. Rev. D* **93**, 114508 (2016), [Erratum: *Phys. Rev. D* **105**, 079902 (2022)], [arXiv:1604.03530 \[hep-ph\]](#).
- [115] C. Alexandrou *et al.*, *Phys. Rev. D* **98**, 074502 (2018), [Erratum: *Phys. Rev. D* **105**, 019902 (2022)], [arXiv:1807.08357 \[hep-lat\]](#).
- [116] M. Niehus, M. Hoferichter, and B. Kubis, *JHEP* **12**, 038 (2021), [arXiv:2110.11372 \[hep-ph\]](#).
- [117] R. L. Workman *et al.* (Particle Data Group), *PTEP* **2022**, 083C01 (2022).
- [118] F. Campanario, H. Czyż, J. Gluza, T. Jeliński, G. Rodrigo, S. Tracz, and D. Zhuridov, *Phys. Rev. D* **100**, 076004 (2019), [arXiv:1903.10197 \[hep-ph\]](#).
- [119] F. Ignatov and R. N. Lee, *Phys. Lett. B* **833**, 137283 (2022), [arXiv:2204.12235 \[hep-ph\]](#).
- [120] J. Monnard, Ph.D. thesis, Bern University (2020), <https://boristheses.unibe.ch/2825/>.
- [121] G. Abbiendi *et al.*, (2022), [arXiv:2201.12102 \[hep-ph\]](#).
- [122] D. Stamen, T. Isken, B. Kubis, M. Mikhasenko, and M. Niehus, *Eur. Phys. J. C* **83**, 510 (2023), [Erratum: *Eur. Phys. J. C* **83**, 586 (2023)], [arXiv:2212.11767 \[hep-ph\]](#).
- [123] C. Hanhart, *Phys. Lett. B* **715**, 170 (2012), [arXiv:1203.6839 \[hep-ph\]](#).
- [124] S. Ropertz, C. Hanhart, and B. Kubis, *Eur. Phys. J. C* **78**, 1000 (2018), [arXiv:1809.06867 \[hep-ph\]](#).
- [125] L. von Detten, F. Noël, C. Hanhart, M. Hoferichter, and B. Kubis, *Eur. Phys. J. C* **81**, 420 (2021), [arXiv:2103.01966 \[hep-ph\]](#).
- [126] R. Omnès, *Nuovo Cim.* **8**, 316 (1958).
- [127] J. J. Sakurai, *Currents and Mesons* (University of Chicago Press, Chicago, 1969).
- [128] F. Klingl, N. Kaiser, and W. Weise, *Z. Phys. A* **356**, 193 (1996), [arXiv:hep-ph/9607431](#).
- [129] C. Bouchiat and L. Michel, *J. Phys. Radium* **22**, 121 (1961).
- [130] S. J. Brodsky and E. de Rafael, *Phys. Rev.* **168**, 1620 (1968).
- [131] V. M. Aul'chenko *et al.* (SND), *J. Exp. Theor. Phys.* **121**, 27 (2015), [*Zh. Eksp. Teor. Fiz.* **148**, 34 (2015)].
- [132] M. N. Achasov *et al.* (SND), *Eur. Phys. J. C* **80**, 993 (2020), [arXiv:2007.14595 \[hep-ex\]](#).
- [133] B. Aubert *et al.* (BaBar), *Phys. Rev. D* **70**, 072004 (2004), [arXiv:hep-ex/0408078](#).
- [134] M. N. Achasov *et al.* (SND), *Phys. Rev. D* **63**, 072002 (2001), [arXiv:hep-ex/0009036](#).
- [135] M. N. Achasov *et al.* (SND), *Phys. Rev. D* **66**, 032001 (2002), [arXiv:hep-ex/0201040](#).
- [136] M. N. Achasov *et al.* (SND), *Phys. Rev. D* **68**, 052006 (2003), [arXiv:hep-ex/0305049](#).
- [137] R. R. Akhmetshin *et al.* (CMD-2), *Phys. Lett. B* **364**, 199 (1995).
- [138] R. R. Akhmetshin *et al.* (CMD-2), *Phys. Lett. B* **434**, 426 (1998).
- [139] R. R. Akhmetshin *et al.* (CMD-2), *Phys. Lett. B* **578**, 285 (2004), [arXiv:hep-ex/0308008](#).
- [140] R. R. Akhmetshin *et al.* (CMD-2), *Phys. Lett. B* **642**, 203 (2006).
- [141] A. Cordier *et al.* (DM1), *Nucl. Phys. B* **172**, 13 (1980).

- [142] A. Antonelli *et al.* (DM2), *Z. Phys. C* **56**, 15 (1992).
- [143] S. I. Dolinsky *et al.*, *Phys. Rept.* **202**, 99 (1991).
- [144] G. D’Agostini, *Nucl. Instrum. Meth. A* **346**, 306 (1994).
- [145] R. D. Ball, L. Del Debbio, S. Forte, A. Guffanti, J. I. Latorre, J. Rojo, and M. Ubiali (NNPDF), *JHEP* **05**, 075 (2010), [arXiv:0912.2276 \[hep-ph\]](#).
- [146] C. Amsler *et al.* (Crystal Barrel), *Phys. Lett. B* **311**, 362 (1993).
- [147] M. Hoferichter, G. Colangelo, B.-L. Hoid, B. Kubis, J. Ruiz de Elvira, D. Schuh, D. Stamen, and P. Stoffer, (2023), [arXiv:2307.02532 \[hep-ph\]](#).